DESIGN OF A SURFACE PLASMON RESONANCE BASED CHEMICAL AND BIO MOLECULAR SENSOR

by

Saimon Bin Islam (152405)

A.N.M. Iftekher (152461)

Kazi Rakibul Hasan (152469)

Md Julkar Nayen (152479)

A Thesis Submitted to the Academic Faculty in Partial Fulfillment of the Requirements for the Degree of

BACHELOR OF SCIENCE IN ELECTRICAL AND ELECTRONIC ENGINEERING

Department of Electrical and Electronic Engineering

Islamic University of Technology (IUT)

Gazipur, Bangladesh

November 2019

DESIGN OF A SURFACE PLASMON RESONANCE BASED CHEMICAL AND BIO MOLECULAR SENSOR

Supervised by:

_____

Prof. Dr. Mohammad Rakibul Islam

Supervisor and Professor,

Department of Electrical and Electronic Engineering,

Islamic University of Technology (IUT)

Boardbazar, Gazipur- 1704.

Date: ……

ABSTRACT

Many researchers have already proved their excellence in the fields of SPR based PCF sensor research work. In the last years, they have proposed great designs with high amplitude sensitivity. But the challenge for designing is that most of the designs exhibit high sensitivity with high loss or they exhibit low sensitivity with low loss. And most importantly the designs become complex in order to achieve high sensitivity. We tried to remove these restrictions and gain high sensitivity with a low loss in simple design where we succeeded. For our thesis paper, we proposed a circular shaped PCF sensor using the principles of SPR. In our proposed design, we compared between circular, elliptical and rectangular airholes for the same design and explored the best results for further investigation. The proposed design is surrounded by a thin Perfectly Matched Layer (PML). A thin gold layer is used as the plasmonic material. TiO_2 layer is also used for better adhesion of the gold layer. COMSOL Multiphysics 5.3a and MATLAB was used for the research work. The technique used for the exploration is Finite Element Method (FEM). The proposed design shows highest confinement loss of 340dB/cm and maximum amplitude sensitivity of 1189.46 RIU^{-1}. The wavelength sensitivity of the design is 13,000 nm/RIU. The design also achieved a sensor resolution of 7.69×10^{-6} which is remarkable. The investigation process covers a wider range of optical spectrum from 0.59 μm to 1 μm. The Refractive Index (RI) of the proposed design ranges from 1.33 to 1.4. For its high amplitude sensitivity and relatively low loss, the proposed design can be used for medical and bio-chemical research.

ACKNOWLEDGEMENT

All praise to the almighty Allah (SWT). By the grace of Him, we were able to complete our assigned thesis with astounding results. We would also like show our gratitude and thank our thesis supervisor Md. Rakibul Islam, Professor Department of Electrical and Electronic Engineering, Islamic University of Technology for his continuous support, helpful attitude, careful guidance, friendly manner and most importantly his constant patience during the learning phases. His helpful attitude towards us helped us to carry on with our thesis work in a speedy manner and helped us to finish the work in time.

We would also like to thank all the teachers of Electrical and Electronic Department for their valuable suggestions and constructive criticism during this research work. Their helpful attitude inspired us during the research work.

Also, this research work wouldn't have been completed without the continuous support and encouragement from our parents who take our side always whatever we try to do. Finally, last but not the least for all the seniors, juniors and well-wishers.

Table of Contents

LIST OF FIGURES

LIST OF TABLES

LIST OF ABBREVIATIONS

PCF	:	Photonic Crystal Fiber
SPR	:	Surface Plasmon Resonance
SPW	:	Surface Plasmon Wave
SP	:	Surface Plasmon
SPP	:	Surface Plasmon Polariton
RIU	:	Refractive Index Unit
RI	:	Refractive Index
NIR	:	Near-infrared Region
EMI	:	Electromagnetic Interference
TIR	:	Total Internal Reflection
TE	:	Transverse Electric
TM	:	Transverse Magnetic
FEM	:	Finite Element Method
MM	:	Multipole Method
PML	:	Perfectly Matched Layer
PMC	:	Perfectly Magnetic Conductor
OFC	:	Optical Fiber Conference
PBG	:	Photonic Band Gap
HNL-PCF	:	Highly nonlinear PCF
IG-PCF	:	Index-Guiding Fibers
PBG-PCF	:	Photonic Bandgap Fibers

HA-PCF	:	Hole Assisted PCF
HC-PCF	:	Hollow Core PCF
HIC-PCF	:	High Index Contrast PCF
HNA	:	High Numerical Aperture
LMA	:	Larger Mode Area
AG	:	Air guiding
THz	:	Terahertz
SNR	:	Signal to noise ratio
LPG	:	Long period grating
FBG	:	Fiber Bragg grating
SERS	:	Surface Enhances Raman Scattering
AS	:	Amplitude Sensitivity
WS	:	Wavelength Sensitivity
LSPR	:	Localized Surface Plasmon Resonance
EML	:	Effective Material Loss
ITO	:	Indium Tin Oxide
TNT	:	Tri Nitro Toluene
CL	:	Confinement Loss
TC-PQF	:	Trapezoidal channel photonic quasi-crystal fiber
TiO_2	:	Titanium dioxide

LIST OF SYMBOLS

ϵ_0,	relative permeability
μ_0,	permittivity in free space
n_{mat}	refractive index of the material
E	modal electric,
α_{eff}	bulk material absorption loss
S_z	z-component of the poynting vector
f	frequency of the guiding light,
c	speed of light in vacuum
$\mathrm{Im}(n_{eff})$	imaginary part of the effective index of the guided mode
n_x and n_y	refractive indices of two orthogonal components of the polarization maintaining wave
A_{eff}	effective modal area
R	bending radius
n_{co}	refractive indices of the core
n_{cl}	refractive indices of the cladding
n_{eff}	effective refractive index,
$\omega = 2\pi f$	angular frequency
$I(r) = \lvert E_t \rvert^2$	transverse electric field intensity in the cross section of the fiber
γD	Damping frequency
ω_D	Plasma frequency
ϵ_∞	Permittivity at high frequency
ε_∞	Intraband dielectric constant

$\Delta\epsilon$	weighting factor
Ω_L	Oscillator strength
d_c	diameter of the central air hole
r	radii of air holes
t_g	Thickness of gold
t_{Ag}	Thickness of silver
t_t	TiO_2 film thickness
n_a	Refractive index
Λ	Pitch
n_c	Number of core air holes
ε	Intraband dielectric constant
Γ	Damping coefficient
m_e	Free electron mass
n_t	Refractive index of ITO
λ	Wavelength
ε_{Ag}	Relative permittivity of silver
ω	resonant frequency
ε_∞	Intraband dielectric constant at infinity

Chapter 1: Introduction

1.1 Background

Since last few decades, optical biosensors are widely used to monitor and analyze the molecular interactions. Optical sensors have gained enormous attention for its easy instant detection capability due to advance optical instrumentations. In the late 1980s, first optical biosensor had been commercialized. The basic principle behind any optical sensor is related with the light matters where the light intensity or electromagnetic fields change due to the presence of samples. A sophisticated device which is able to convert the light rays into electrical signals and thus can be made to detect the change and response of ambient condition or to measure the intensity of electromagnetic waves called an optical sensor. So far, a number of optical sensor techniques are available such as micro-ring resonator, surface plasmon resonance, resonant mirrors, photoluminescence and evanescent wave absorption spectroscopy

Optical Chemical and Biomolecular sensors based on Surface Plasmon Resonance (SPR) present one of the most advanced label-free optical sensing technologies [1]. Their ability to analyze and monitor the interaction between a molecule immobilized on the surface of the sensor and the interacting molecular partner in a solution have made SPR sensors a very powerful optical sensor for biomolecular interaction analysis and biomolecular research in general [2].

Optical sensors based on surface plasmon resonance works initially by generating the surface plasmon wave (SPW) which can be done by matching the incident light frequency of the p-polarization or transverse magnetic (TM) surface electrons resulting the free electrons of the metal surface start to resonate which propagates along the metal-dielectric interface. SPR sensors require a metallic component carries large number of free electrons. These free electrons provide the real part of a negative permittivity which are essential for plasmonic materials. Conventional prism based Kretschmann set-up is widely used for SPR sensor where the p-polarization or transverse magnetic light is incident on a prism coated with plasmonic materials (Au, Ag, Cu, etc.) and generates the surface plasmon polaritons (SPP) wave that propagate along the surface (Gupta & Verma, 2009). A change in dielectric refractive index causes a change in propagation constant of the surface plasmon (SP) mode. This change consequently affects the coupling condition of the

light wave and the SP wave, and the changes can be detected and analyzed from one of the characteristics of optical wave interacting with the SP mode.

The past years have witnessed growing number of studies reporting the use of SPR, its application, method of implementation, SPR technology, with over 1000 new publication each year [3] .So far SPR sensors have been used for detection of chemical and biological substances of medical, environmental or military interests .Several successful instruments platforms have been reported since the introduction of SPR biosensors [4]. Variety of available commercial SPR sensors include high-resolution sensor systems for the most demanding research into biomolecular interactions as well as more simplified and cost-effective solutions for fast detection of selected species [5].

The need for simultaneous monitoring of hundreds or even thousands of biomolecular interactions emerged in areas of medical diagnostic [6], drugs development [7] and food safety and security. Biomolecular interactions are the key factors of drug-discovery technique. By analyzing the molecular interactions, it is possible to diagnose the facts about the diseases. High-performance SPR platforms with angular or wavelength spectroscopy were demonstrated to offer the potential for increased throughput [8], however the complexity and cost of these sensor system increase proportionally to the number of channels.

Due to having a wide field of applications and flexibility in implementation, high sensitivity (even for a very small change of condition and properties of materials) and a future scope of study, optical sensors based on SPR phenomenon are currently a very attractive sector to conduct research work.

1.2 Problem Statement

Being an attractive field of research, several designs for SPR based optical sensor had been implemented by the researcher and noticeable development had been observed. Though internal sensing technique gives higher sensitivity than external one, it is costly and has a complex structure. Thus, most of the reported sensors structure that were reported are difficult to be fabricated due to selective coating of metal layers and liquid infiltration inside the air-hole surface and the performance of these reported sensors are observed by following the inside sensing. Several PCF SPR sensors were reported also where the metallic and sensing layer are placed

outside the fiber structure to simplify the sensor configuration. However, to control the light propagation in specific direction to enhance the evanescent field, these sensors introduced non-circular air-holes (Akowuah et al., 2012; Otupiri, Akowuah, & Haxha, 2015), and also several small air-holes are selectively placed in the specific position which makes the sensors structure complex in terms of fabrication (Dash & Jha, 2014a; Otupiri et al., 2014) operation. On the contrary, achieving high sensitivity with having a comparatively low loss is still a challenge for these sensors. Thus, so far, the limitations that were observed for the SPR based optical sensors are as follows:

- ✓ Fabrication difficulty due to internal sensing technique
- ✓ Weak evanescent field
- ✓ Design complexity to achieve high sensitivity
- ✓ High loss

1.3 Research Objective

Optical fiber was initially used mainly for the transmission purposes. Thus, some of the researching challenge was to achieve high birefringence with minimum effective material, confinement loss, dispersion, bending loss, scattering loss etc. The Eml value obtained lowest so far is 0.009 [9]. Thus, further decreasing the value is really hard and most importantly not necessary because of complexity in designing. Same goes for the confinement loss and other parameters. Thus, this field has become saturated with almost no scope for further improvement and researchers are now a days giving less attention in this area because SPR is more promising and has a lot of rooms to research than transmission applications.

The aim of our thesis was to study recent reported SPR based designs and make a review based on those papers to understand SPR phenomenon and its related term properly and to build our own design based on that in order to provide a reliable solution for the above-mentioned problems.

In particular, the objectives of the research are follows:

- ✓ Conducting a review on the reported design of SPR based sensors

- ✓ Proposing a design which follows external sensing approach and can guide strong evanescent field
- ✓ Making the design implementation compatible with the contemporary fabrication processes
- ✓ To analyze the performance of the proposed sensors based on wavelength and amplitude interrogation method.
- ✓ To achieve a high sensitivity with having a low confinement loss

1.4 Motivation

Surface plasmon resonance is a quantum optical effect that enables the sensitive detection of biomolecular interactions directly without having to label probe molecules with fluorescent markers or the use of color changing substrates which enables a lot of applications for it. For example, it can do an immediate test for the presence of any growth hormone in milk by sensing interactions with hormones complementary antibody. It can be used to perform DNA and RNA assays by detecting interactions of the complementary base pairings in real time. It can rapidly test for the presence of viruses like dengue in blood samples by sensing reactions with virus specific antigens.

The heart of a surface plasmon resonance-based sensor is a gold film, thinner than the width of most viruses. It performs biology on one side and physics on the other. On the biology side, biomolecules are mobilized on the surface of the gold film act as molecular probes and on the physics side, infrared light creates a resonance with surface plasmons in the film creating a minimum and reflected light intensity at a particular angle. When target molecules react with the probes this effects the optical properties and the minimum angle changes. The reflected light profile is turned into an electrical signal by a linear ray detector. The position of the minimum tracts the biochemical interactions.

Samples of only a few nano grams of molecules can create a clear reaction graph with angle vs time. Tests can be completed in two to ten minutes. Thus, it is an established analysis method. The only alternatives are the commercial instruments that cost tens of thousands of dollars both in construction and maintenance. SPR technology can be democratized, making available to everyone within instrument that is fast, accurate and easy to use. It can be used to assay antibody-antigen,

bacteria, virus, DNA, RNA, mRNA, hemoglobin, hormone, protein etc. It can also be further used in near future in physics, electronics and software.

So, one can focus on its applications in biological sector, physics, environmental science and education. Having a vast filed to study and to conduct research with it in physics or biology or chemistry and much room to improve, SPR technology is one of the most promising research area at present.

1.5 Thesis Framework

This thesis report is organized into six chapters. A brief overview of the chapters are given in this section.

Chapter 2 provides the basic introduction of photonic crystal fiber (PCF) and its evolution in optical fiber technology. Different types of PCF that are currently being used is discussed with mentioning the differences of PCF based fiber from the conventional one. The structural properties of PCF based fiber following by the type of optical fiber sensors and different sensing types are also discussed in detail. Finally, the method, algorithms which are used to simulate the result and the software that is used are presented briefly.

Chapter 3 presents a detail information of what is SPR, its background history, how SPR forms through by Surface plasmon wave (SPW), Resonance and generates surface plasmon polariton with the help of evanescent field. This section is concluded with describing the different structural properties and their impact on the sensor.

In Chapter 4, we presented a detail analyzation on the implemented designs that are reported recently. The designs are categorized based on the its geometrical structure and its sensing approach. Two sample designs are implemented to discuss and compare different designs with our understandings from the analyzation.

Chapter 5 is the main core part of our thesis, proposed a SPR based optical fiber design which can fulfil our research objective. Three designs are presented and a comparative analysis among them is provided. All the results that are obtained from the simulation of the implemented design are plotted and mentioned and compared with the previously reported designs.

Chapter 6 presents the conclusion, socio-economic impact and other proposed future works.

Chapter 2: Technical Background of Optical Fiber Transmission and sensing

2.1 Overview

In this chapter we presented a brief discussion of Photonic Crystal Fiber (PCF) , classification of PCF, difference between PCF based fiber and conventional fiber, light guiding mechanism of PCF. We also discussed some structural properties like EML, confinement loss, birefringence, bending loss, chromatic dispersion and effective area. Usage of optical fibers as sensors, different kinds of sensing like, refractive index sensor, microband fiber optic sensor, surface enhanced Raman Scattering and surface plasmon sensors, different methods of sensing and some simulations are also discussed in different sub-section.

2.2 Evolution of Photonic Crystal Fiber

Photonic Crystal fibers (PCF) are fibers with a periodic transverse microstructure. In 1978, the idea of photonic crystal fiber was presented for the first time by Yeh et al. They proposed to clad a fiber core with Bragg grating, which is similar to 1D photonic crystal. A 2D photonic crystal fiber with an air-core was invented by P. Russell in 1992. And the first PCF was reported at the Optical Fiber Conference (OFC) in1996. PCFs have been in practical existence since 1996 as low loss waveguides. It took four years of technological development for the initial demonstration and since then the techniques of fabrications becoming more and more complicated. Manufacturing the microstructure in air-glass PCF to accuracies of 10 nm on the scale of 1 um is now possible. Now we can control some key properties like, birefringence, dispersion, nonlinearity and the width and position of the Photonic band gap. PCF has a great range of possibilities by introducing new features like low-loss guidance in a hollow core.

2.2.1 PCF in Brief

The kind of optical fiber that uses photonic crystals to form the cladding around the core of the cable is called Photonic Crystal Fiber (PCF). Photonic Crystal is a low loss dielectric medium that is constructed using a periodic array of microscopic air holes and it goes along the whole fiber length [10]. Light is trapped in the core in PCF and it gives a better wave guide to photons than standard optical fiber. The core guidance of the optical signal is provided by a solid silica core in

PCF. This core is surrounded by periodic air-hole array in the cladding. As the effective cladding index is lower than the core refractive index, light signal can be guided by total internal reflection along the silica defect core. The air-holes add up to the low index cladding and the core is usually formed by making a larger air hole in its position or removing an air hole from the center of the structure. PCFs have some design freedom, like, core radius, number of rings, air hole diameter and pitch (air hole to hole diameter). Application of guiding properties can be gained by modulating these parameters as the guiding properties of optical fibers depend on the refractive index and refractive index of PCFs depends on those design freedoms [11].

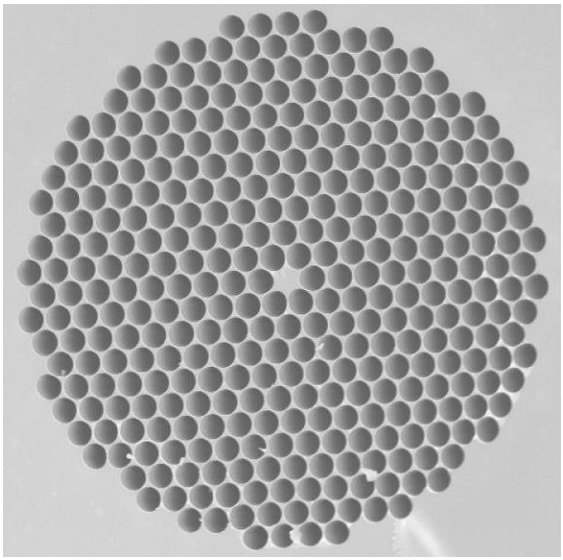

(a)

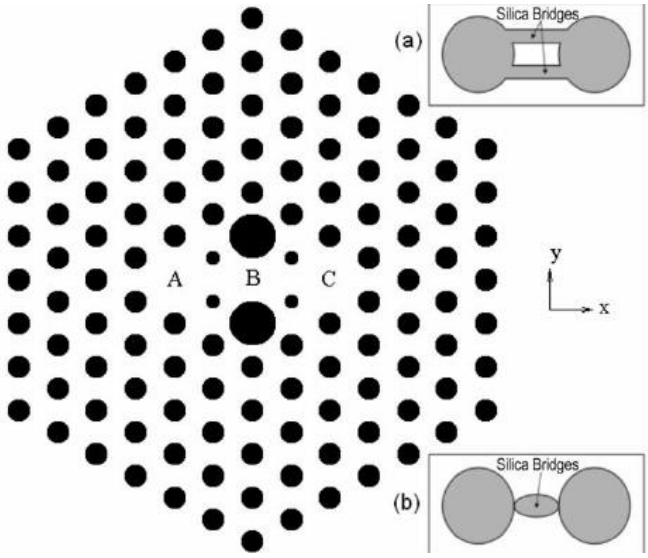

(b)

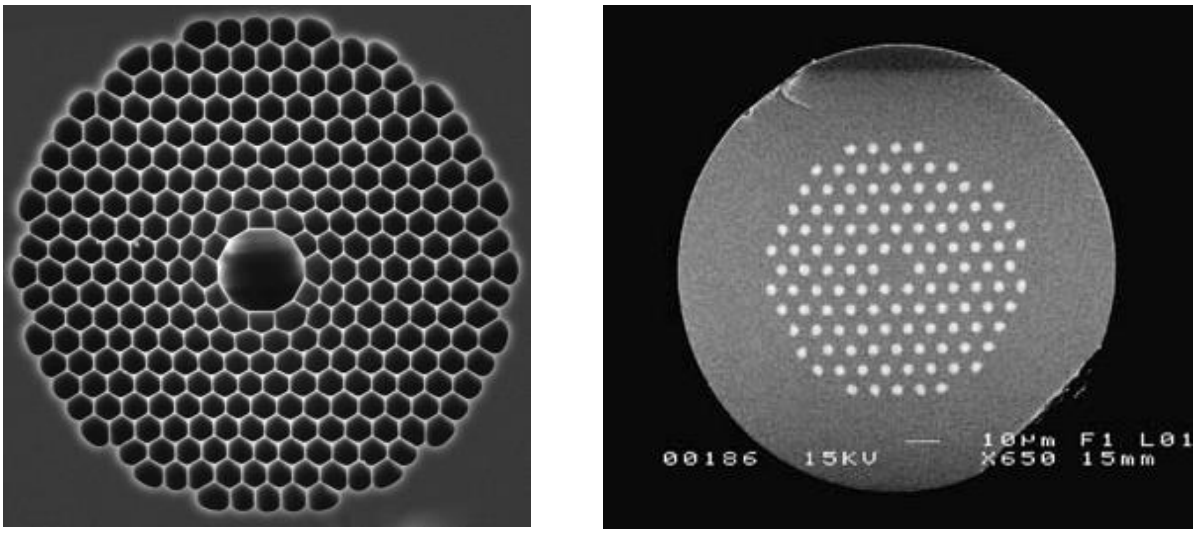

(c) (d)

Fig.2.1: Scanning electron micrographs of different PCF cross-sections. (a) a large-mode-area air-silica endlessly single-mode PCF, (b) an air-silica highly birefringent PCF, (c) an air-silica air-core PBF, (d) an all-solid PBF

2.2.2 Classification of PCF

PCFs can be classified into several types. The classification depends on the structures, fiber parameters and specific guiding properties [12]. PCFs are generally divided into two main categories: Index-Guiding Fibers (IG-PCF) and Photonic Bandgap Fibers (PBG-PCF).

Index Guiding PCFs or IG-PCF are of several types such as, Highly Nonlinear fibers or HNL fibers (which has a very small core dimensions to ensure tight mode confinement), High Numerical Aperture fibers or HNA fibers (which has a microstructure cladding and a ring of air holes surrounds the cladding) and Larger Mode Area fibers or LMA fibers (which has a larger dimension of the core and small refractive index to ensure a larger effective area). Hole Assisted PCFs (HA-PCFs) are another type of IG-PCF when IG-PCFs have a doped core (which has high index doped silica) and a holey cladding.

Photonic Bandgap Fibers (PBG-PCFs) are of different classes such as, Air-Guiding fiber (AG fiber) or Hollow Core (HC fiber) and LIC fibers or Bragg fibers.

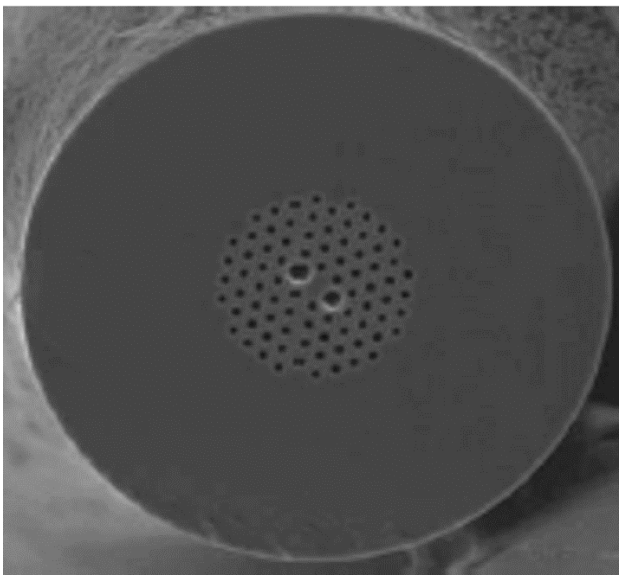

(a)

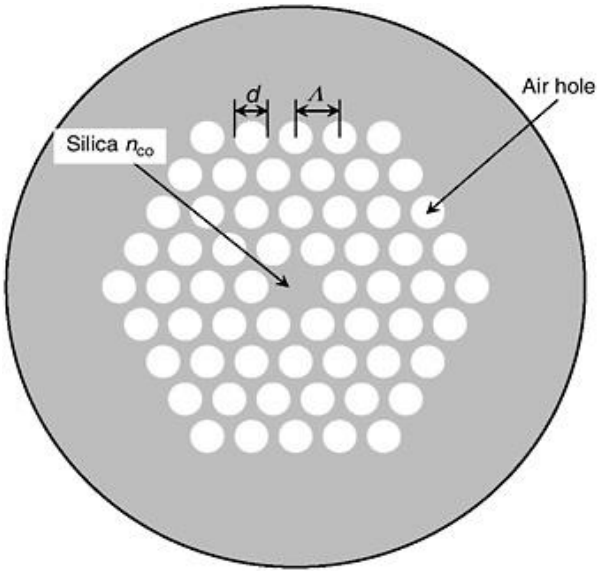

(b)

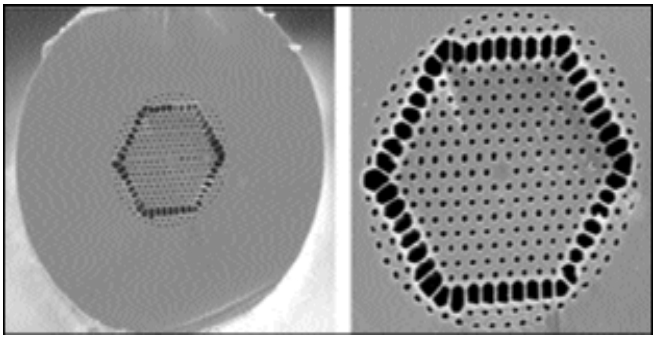

(c)

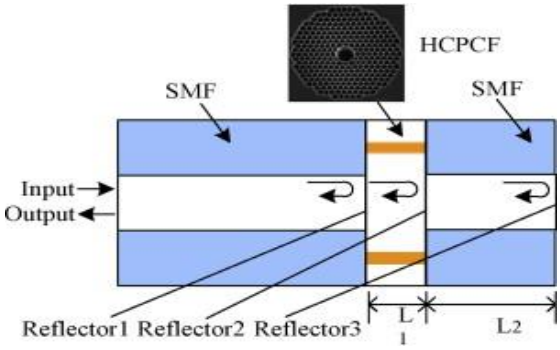

(d)

Figure 2.2: Types of PCFs (a) PM-PCF, (b) HA-PCF, (c) HNA-PCF and (d) Bragg Fiber- a special type of HC-PCF [13].

2.2.3 Difference of PCF based fiber and conventional Fiber

A conventional optical fiber has a core that has a higher refractive index than the cladding. A high refractive index material is doped in the core region to make its

refractive index higher than the silica cladding. Germanium is usually used for increasing the refractive index of the core and Fluorine is usually used for decreasing the refractive index.

On the contrary, PCF is made of a single material which contains very small air-holes in a silica background. In conventional fibers, index contrast between the core and the cladding is very low but in case of PCF, this index contrast is pretty high and manageable. This is achieved by tuning the difference between two fibers which makes significant differences in their optical properties [14]. PCF shows super low or high nonlinearities, wider single mode operation, high birefringence, flat dispersion any many others [15].

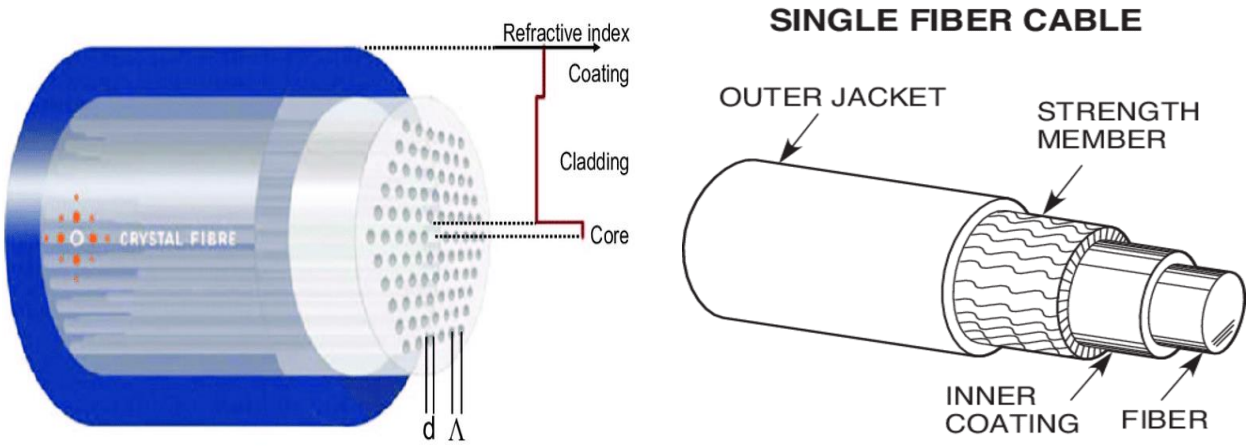

Figure 2.3: cross sections and index-profiles of (a) PCFs and (b) Ordinary fibers [16].

2.2.4 Light guiding Mechanism of PCF

The light guiding of PCF is based on two mechanisms, Total Internal Reflection (TIR) mechanism and Photonic Bandgap (PBG) mechanism [17]. If the light is guided PCF using TIR mechanism, it is called Index-Guided PCF (IG-PCF) or High Index Contrast PCF (HIC-PCF). On the contrary, if the light is guided using PBG mechanism, it is called Photonic Bandgap PCF (PBG-PCF) or Hollow Core PCF (HC-PCF).

IG-PCFs usually exclude a single air-hole from the structure and this kind of PCFs also have a doped core with a high index core. In both cases, the core must have a high refractive index ($n_{core} > n_{cladding}$) than the refractive index of cladding. PGB-PCFs have a hollow core. Generally, the hollow core is made by creating a larger air-hole in the center of the structure.

2.3 Structural properties of Optical Transmission Fiber

Structural properties of optical fiber are represented in this section. Structural properties include EML, confinement loss, birefringence, bending loss, chromatic dispersion and effective area.

2.3.1 Effective Material Loss

For long-haul transmission, in an optical fiber, the important parameter that must be remembered is effective material loss (EML). It is due to EML that signal is dropped constantly and cannot travel very long distance. The EML indicates the total amount of light energy that is absorbed by the core material itself. The equation that defines the EML is [18]

$$\alpha_{eff} = \sqrt{\frac{\epsilon_0}{\mu_0}} \left(\frac{\int_{A_{mat}} n\alpha_{mat} |E|^2 \, dA}{2\int_{All} S_z dA} \right) \tag{2.1}$$

where, ϵ_0, μ_0, n_{mat} are relative permeability, permittivity in free space and refractive index of the material respectively. E is the modal electric, α_{eff} is the bulk material absorption loss and S_z is the z-component of the pointing vector and $S_z = 1/2(\mathbf{E} \times \mathbf{H}) * z$ [18].

Higher core porosity causes EML to decrease; this is because higher porosity means few materials inside the core, so there is less absorption loss. On the other hand, at fixed porosities, as core diameter increases, EML also increases. Also, as frequency increases EML also increases, because the lower frequency light wave propagates through the air holes of the cladding region and not perfectly confined in the core region [18].

2.3.2 Confinement Loss

A THz PCF's confinement loss is a crucial guiding property as it limits the duration of the real THz transmission system. Limited air holes in the center locale prompt leakage of optical mode from the inner center region to outside air gaps and this is inevitable resulting in confinement loss [19]. It is described as the reduction resulting from the finite magnitude of the regular cladding [20]. Confinement loss can be altered with regard to parameters such as amount of air holes, diameter of the air hole, number of layers and pitch. It is defined by the equation:

$$\alpha_{CL} = 8.686\left(\frac{2\pi f}{c}\right)\mathrm{Im}\left(n_{eff}\right) \tag{2.2}$$

where, f is the frequency of the guiding light, c is the speed of light in vacuum and Im(n_{eff}) is the imaginary part of the effective index of the guided mode [18].

Confinement loss is inversely related to frequency; this is because high frequency spectrum and limited core porosity lead to more concentrated light in the core. Confinement loss reduces as the core diameter is incremented and rises when the porosity is increased. The reason behind this phenomenon is that when core-cladding refractive index distinction scales up n_{eff} decreases and subsequently forces light to stay in the core when the core is expanded. In contrast, as core porosity increases the index difference decreases which causes the light to spread gradually to the cladding region, thus boosting the confinement loss [21].

2.3.3 Birefringence

Birefringence is an important property in fiber optics as well as in many applications where birefringence is used to support light in a linear polarization state. Generally, materials with uniaxial anisotropy, the axis of symmetry or the optical axis of a specific material that has no corresponding axis in the plane perpendicular to it, exhibits this optical phenomenon. For an irregular light rays, linearly polarized light rays in parallel and perpendicular direction will have uneven refractive indices, n_e and n_o, respectively. When a non-polarized light beam moves through fabric with an acute non-zero angle to the optical axis, the perpendicularly polarized element may experience refraction at an angle as per ordinary refractive law and its reverse component at a non-standard angle shown by the distinction between the two efficient refractive indices called as the birefringence magnitude [20]. The birefringence is expressed as [22]

$$B = \left|n_x - n_y\right| \tag{2.3}$$

where n_x and n_y are the refractive indices of two orthogonal components of the polarization maintaining wave. Birefringence improves with an increase in frequency because it increases the index contrast between orthogonal polarization modes. It is also noted that the quantity of birefringence declines at greater porosity values because increase in porosity allows more power

to propagate outside the core region, which ultimately reduces the index contrast between the polarization modes [22].

2.3.4 Bending Loss

Bending loss is a very crucial parameter for the practical implementation of THz waveguide. The bending loss can be quantified by using the following formula [14]

$$\alpha_{BL} = \frac{1}{8}\sqrt{\frac{2\pi}{3}}\frac{1}{A_{eff}}\frac{1}{\beta}F\left[\frac{2}{3}R\frac{(\beta^2-\beta_{cl}^2)^{3/2}}{\beta^2}\right] \tag{2.4}$$

where, A_{eff} and R are the effective modal area and the bending radius, respectively. $F(x) = x^{-1/2}e^{-x}$, $\beta_{cl} = 2\pi n_{cl}/\lambda$, $\beta = 2\pi n_{co}/\lambda$; where n_{co} and n_{cl} are the refractive indices of the core and cladding, respectively.

Bending loss decreases with increase in frequency. It is high for large values of porosity and smaller bending radii because the fiber does not trap enough light inside the core when more bent or the index contrast is further lowered by the porous air holes in the core [19]. Moreover, bending loss is minor compared to other losses.

2.3.5 Chromatic Dispersion

Chromatic dispersion happens due to pulse expansion and is one of the primary problems in fiber optic communication system. In the material or in the waveguide, dispersion can take place [20]. However, owing to the steady refractive index of Topas within the frequency band under account, the material dispersion may be ignored since the dispersion of light in the material is negligibly low. High waveguide dispersion may improve the rate of bit error during transmission and should usually be kept low for reliable transmission [21]. Dispersion parameter, β_2, of the suggested fiber can be calculated using the following expression [21]

$$\beta_2 = \frac{1}{c}\left(2\frac{dn_{eff}}{d\omega} + \omega\frac{d^2n_{eff}}{d\omega^2}\right) \tag{2.5}$$

where n_{eff} is the effective refractive index, c is the speed of light in vacuum, and $\omega = 2\pi f$ is the angular frequency. Its unit is ps/THz/cm.

Changes in pitch and radius have an impact on the effective refractive index, resulting dispersion to vary. Dispersion increases for the use of larger pitch value and it decreases for smaller pitch values [23]. It should also be noted that dispersion decreases with an increase in frequency [24]. High dispersion restricts the rate of data transmission and effective transmission so it's an issue and it must be as small as possible.

2.3.6 Effective Area

The effective modal area is a key property of photonic crystal fiber. For communication and other high-power applications, PC-PCFs with a big effective modal region are essential. The effective modal area is to quantify the total region played by the basic mode and it may be evaluated by using the following formula

$$A_{eff} = \frac{\left[\int I(r)\,dr\right]^2}{\left[\int I(r)\,dr\right]^2} \tag{2.6}$$

Here, $I(r) = |E_t|^2$ is the transverse electric field intensity in the cross section of the fiber. Effective area reduces with an increase in frequency as the mode gradually extends with growing frequency towards the cladding region, thus decreasing the area of the fiber occupied by the basic mode [21].

2.4 Optical Fiber as Sensors

In this modernized world, the necessity to monitor environmental factors, like, humidity, temperature, stress, concentration of chemical or biological species is increasing rapidly.

Optical fiber sensing is in competition with other sensing technologies but it is preferred for following reasons:

- ✓ Remote sensing: a segment of fiber can be used as a sensor gauge with a long segment of another or same fiber that transmits the sensing information to a remote

station. Optical fibers give lower signal loss and can maintain a high signal-to-noise ratio (SNR) compared to other sensors.

- ✓ Versatile installation: as optical fibers are very small in size; it enables easy installation in limited spaces.
- ✓ Easier transportation: optical fibers are very lightweight and so they are very easy for transportation in remote locations.
- ✓ Accuracy: optical fiber sensors provides very accurate results as they are free from electromagnetic interference.
- ✓ Detection of extremely small targets: the extremely compact sensor head allows easy detection of small targets.
- ✓ Excellent environmental resistance: as no electrical current flows through the fiber optic cable, the sensor is unaffected by electrical noise. The heat resistant type fibers enable detection in high temperature environments.

Because of these advantages, optical sensors are now replacing conventional sensors. They are also being used in various experimental research tools to get accurate measurements. The use of optical fiber sensors to sense the chemical concentration is started since the 1960s. In general, optical fibers are of two kinds: Intrinsic and extrinsic.

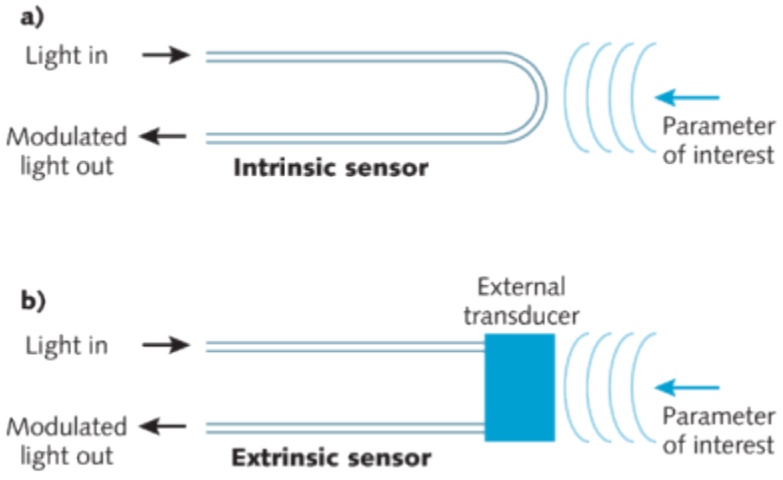

Figure 2.4: a) Intrinsic sensor b) Extrinsic sensor

2.4.1 Intrinsic Sensors

The principle of intrinsic sensor is that the sensing takes place within the fiber itself as shown in figure 2.5(a). The propagating light does not leave the fiber and it is altered by an external phenomenon. This can be tracked by changes in some features like, polarization, wavelength, intensity, phase etc. In intrinsic optical fiber sensors, there are four kinds of general sensor designs. They are: fiber refractometer [25], evanescent-wave spectroscopic [26], active coating [27,28] and active core [29,30].

2.4.2 Extrinsic Sensors

The principle of extrinsic sensor is that the sensing takes place in a region outside the fiber as shown in figure 2.5(b). The usage of optical fiber is only as the mean of light delivery and collection. Another or same fiber can detect and collect back the propagating light that leaves the fiber.

A good example of an extrinsic optical fiber sensor is an optical fiber liquid level sensor. It has been developed in recent years and it is based on the direct interaction between the light and liquid. The most common method that is used in this kind of sensor is to attach a prism to the ends of two single optical fibers [31].

Another example of an extrinsic optical fiber sensor is an optrode. There is a source fiber and a receiver fiber connected to a third optical fiber by a special connector using in the design of optrode [32]. There is a coating of sensitive material on the end side of the third fiber. The chemical that we want to sense interacts with the sensitive end by changing the reflection, absorption and scattering properties or by changing the RI, polarization behavior and luminescence intensity. In this case, the fiber works as a light pipe that transmits to and from the sensing region.

Generally, there are both advantages and disadvantages to using both classes of sensor. Intrinsic sensors are more sensitive and more difficult to refrain from unwanted external disturbances. And on the other hand, extrinsic sensors are less sensitive, easier to use and more easily multiplexed [33].

2.5 Optical Fiber Sensing

Optical fiber sensing can be of many types like refractive index sensing, microbend fiber optic sensing. This section presents the different types of optical fiber sensors based on different types of sensing technique.

2.5.1 Refractive index Sensor

Through the measurement of RI, several different physical and biological parameters and various chemical substances can be detected. This is the motivation for the researchers to give effort in making optical fiber RI sensors. Optical fibers now being used in pollution monitoring in water supply and other public utilities and also monitoring chemical concentration in harsh environments. The proposed design elements for optical fiber RI sensors are fiber gratings [34-36], specialty fibers [37-39] and interferometry [40].

Long period grating (LPG) and Fiber Bragg grating (FBG) are generally used for RI measurement. RI changes are detected from the shifts of the reflection or transmission spectra. This is due to the effect of the external RI on the fiber gratings. LPG sensors have better sensitivity as it couples the light from the core mode to cladding mode. FBG based sensors are less sensitive than LPG sensors. So, to increase sensitivity, the cladding around the FBG is usually thinned [35,36,41]. RI sensors based on fiber gratings are expensive because of the fabrication process.

For biochemical sensing, specialty fibers such as micro-structured fiber [38], cladding stripped fiber [39] and D-shaped fiber [27,42] are being used. Accessing the evanescent field at the interface of fiber core and the surrounding medium is required for these type of optical fiber chemical sensors. To remove a part of the fiber cladding, a precision micro-matching is also required.

There are two beams in an interferometer-based RI sensor [40], one beam is used as the reference and the other beam is exposed to the external medium and serves as the sensing arm. These two arms combined generate an interference pattern. If there is a change in the external RI, the optical path length of the sensing arm is altered and causes a shift in interference pattern. To split the incoming light into two arms, a mechanism is required with the advent of fiber optic couplers.

2.5.2 Microbend Fiber optic Sensors

The principle of microbend fiber optic sensor is intensity of loss through a curved section of an optical fiber [43-46]. When the fiber bend radius is changed, the intensity loss also changes. This makes it possible to deduct the applied force with the change in the transmitted intensity. These approaches are inexpensive and simple. The causes of change of transmitted laser are temperature, change in the bend radius by applied force etc. These changes can be detected and used in sensing. Some existing application of microbend sensors are detection of cracks [46], stress, strain [47], chemical species [48] and pH in a solution [45]. Some other applications are measuring RI of a liquid [49], liquid level in a vessel [50], noise in a combustion engine [51] and humidity [52, 53]. Even though the principle is simple, but the complexities in maintaining and the tiny size of the sensor is still a challenge.

2.5.3 Surface Enhanced Raman Scattering

Surface Enhances Raman Scattering or SERS in short, is a form of Raman spectroscopy which involves the experiment of interacting in some manner with metal surfaces or the samples absorbed to. No metal particles are present and the target analyte interacts directly with the incident electromagnetic field in case of conventional Raman Scattering. In case of surface enhanced Raman scattering, there is a coating of metal colloids around the substrate and the chemical to be examined is on the metal surface. This metal coating creates the surface plasmon resonance on the substrate surface. This substrate surface is responsible for transferring energy through an electric field to the target molecules and it allows inaccessible vibrational structures to be determined. In the case of SERS, the signal is much enhanced than conventional Raman spectroscopy.

SERS sensor is made of a single optical fiber and its end-face is coated with a thin layer of nanoparticles and it is used as a waveguide for the transmission of an excitation laser beam. It results in a high-quality SERS signal. There are a lot of fabrication techniques for optical fiber SERS sensors. They are: an angle-polishing technique of the fiber tip in which the signal can be enhanced by a factor of six [54], a unique optimized fiber tip geometry which helped to improve the sensor's detection limit [55,56], a long optical fiber made of side-polished and end-polished fibers [57].

2.5.4 Surface Plasmon Sensors

For the past few years, there were many applications of fiber-based surface plasmon resonance (SPR) sensors like, SPR sensor configuration with single and multimode and polarization maintaining fibers which is coated with a thin metallic layer [58-61]. A surface plasmon resonance occurs when light is reflected off a thin metal film (e.g. Au, Ag) deposited on a substrate (e.g. glass, prism, quartz) and when the angle of incidence is greater than the angle of total internal reflection (TIR). A small amount of the light energy interacts with the collective oscillation of free electrons in the metal film and reduces the intensity of reflected light. SPR have been attracted a lot of attention in recent years in optical sensing research due to its unique physical properties.

2.6 Methodology and Simulation

In this section, the design methods of the SPR sensor is presented in details. This section also includes the theoretical description of the model in terms of its numerical characterization to match real life operation and also its performance metrices. In this section, all numerical tools used in the realization of the biosensor are also included.

2.6.1 Different Methods

To evaluate the propagation of electromagnetic or acoustic waves through a layered medium, the transfer-matrix method is used in optics and acoustic. Fresnel equation describes the phenomenon of reflection of light forming a single interface between two media. The reflections are partially transmitted and then partially reflected when there are multiple interfaces. Depending on the accurate path length, these reflections can affect constructively or destructively. The overall reflection of a layer structure is the sum of an infinite number of reflections. Maxwell's equations state that there are simple continuity conditions for the electric field across boundaries from one medium to another. The final step of the method is converting the system matrix back into transmission and reflection coefficients.

To solve the Maxwell's equations, a computational technique, plane wave expansion method is used by formulating an eigenvalue problem out of the equation. This method is popular for designing photonic crystal fibers [62]. In calculating modal solutions of Maxwell's equation, plane wave method is very useful. Plane wave method is used in computing over a periodic geometry. It

is a vectoral method and it is directly applied to the fiber design. When characteristic width and center of each chosen with localized function approach, particular knowledge about the solution is not necessary [63].

2.6.2 FEM and Proposition for the use of FEM

Finite element method (FEM) is an arithmetic technique to find estimated solutions of boundary value problems for partial differential equation. In this method, finite elements are used and these are the subdivision of the whole problem domain. It uses variational methods to solve the problem by minimizing an associated error function. By connecting many simple element equations over many small sub-domains, naming finite elements in FEM, a complex equation is guessed over a bigger domain. FEM requires the division of the PCF cross section into mesh within each Maxwell's equation.

The methods have some advantages while analyzing micro-structured fibers. For specific method, there is specific advantage and for our thesis we used FEM method and it accurately represents complex geometry. FEM is a summation of divergent material properties and an easy representation of total solution. To solve complex nonlinear problems, FEM is more suitable [64]. In the presence of layer with strong attenuation, transfer matrix method is numerically usable.

FEM shows its superiority in irregular domains, especially when boundary conditions are involved. The main benefit of FEM is it can deal with both complex 2D and 3D domains [65]. FEM shows great result when the problem needs local mesh refinement. The proposed model has to complete mesh refinement, so, FEM is chosen. The FEM can solve inhomogeneous domains better than homogeneous domains, and this is an advantage. FEM has the ability to model compositionally and geometrically complex problems and it is one of the main reasons for choosing FEM [66].

2.6.3 Implementation of FEM on PCFs

A full vectoral analysis is required for the study of hybrid mode and polarization dependent wave propagation. Considering an optical waveguide with an arbitrary cross section in the x-y plane that has a full vectoral wave equation derived from Maxwell's equation:

$$\nabla \times \left([p] \nabla \times \varphi \right) - k_0^2 [q] \varphi = 0 \tag{2.7}$$

2.6.4 PML and Effective Refractive Index

The additional spaces or domains that do not reflect incident radiation rather absorbs them are called Perfectly Matched Layer (PML). It is a part of the model and it is to made of different absorbing material of various thickness. A matching isotropic permeability and permittivity with the physical medium outside the PML is required such that there are no reflections. By introducing a complex valued coordinate transform under the additional requirement, we can use Maxwell's equation to formulate the PML.

2.6.5 Software Used for Simulation

COMSOL Multiphysics is a powerful software tool and is a cross-platform finite element analysis, solver and Multiphysics simulation software. It allows conventional physics-based user interfaces and coupled systems of partial differential equations. As it can perform modal analysis eigen-frequency and finite element method (FEM) we used this software for the simulation purposes of the SPR based designs.

As this study is fully based on simulation works, all proposed sensors are investigated with the commercial COMSOL 5.3a software and performances are optimized with wavelength and amplitude interrogation methods. The accuracy of the simulation methods are verified with the reported literature before analyzing the proposed sensors. Effective refractive index is the main important thing that is needed from the simulation results for further calculation Proposed PCF SPR sensors are developed by considering the selectively metal coating, liquid infiltration and external sensing problems.

Chapter 3: Surface Plasmon Resonance and SPR Based Optical Fiber Sensors

3.1 Introduction

Surface plasmon resonance (SPR) is an optical-based, label-free detection technology for real-time monitoring of binding interactions between two or more molecules. Being a physical process SPR can occur when plane-polarized light hits a thin metal film under total internal reflection conditions when the resonant oscillation of conduction electrons at the interface between negative and positive permittivity material stimulated by incident light. Binding interactions between a molecule on the sensor surface and its binding partner(s) in solution (mentioned as analyte) are monitored in real-time by SPR. When the molecules bind, the refractive index close to the surface changes causing a shift in the angle of minimum reflected intensity. SPR-based analytical biosensors can be extremely powerful tools for the characterization of molecular interactions. The combination of three individual elements, the detector, the sensor surface and the sample delivery system are critical to the performance of the experiment [67].

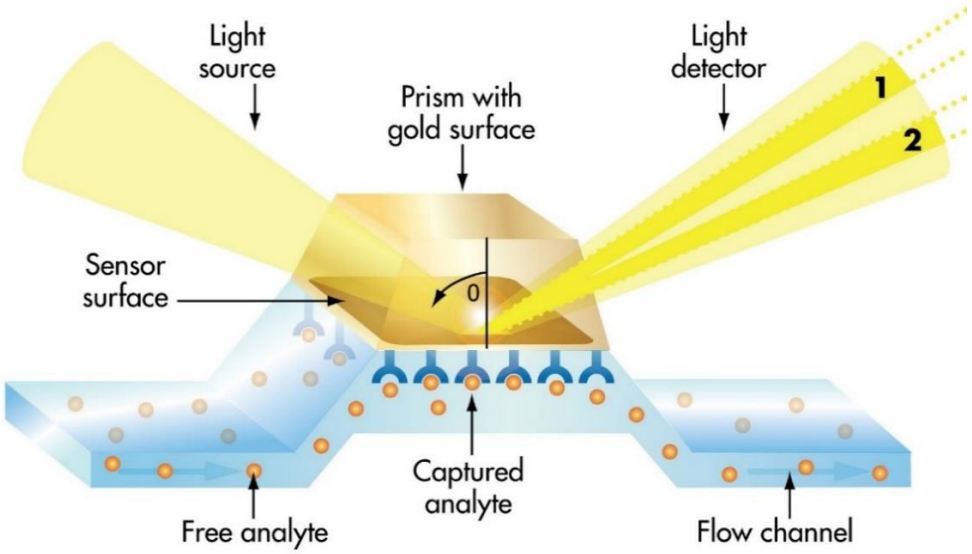

Fig 3.1 Surface Plasmon Resonance

3.2 History

In the late sixties, optical phenomenon of surface plasmons through attenuated total reflection was demonstrated by Kretschmann and Otto [68-70].

Optical excitation of surface plasma waves has two major approaches: attenuated total reflection in prism coupler-based structures and diffraction at diffraction gratings. The application of surface plasma waves for sensing has been pioneered by Nylander and Liedberg [4]. Particularly because of its relative simplicity, this method has been widely applied for characterization of thin films [71-72] and biochemical sensing [73-75].

In the 1980s, SPR and related techniques were applied to the interrogation of thin films and also for biological and chemical interactions [71]. These techniques allow the user to study the interaction between immobilized receptors and analytes in solution, in real time and without labelling of the analyte. By observing binding rates and binding levels, there are different ways to provide information on the specificity, kinetics and affinity of the interaction, or the concentration of the analyte.

In 1980, Pharmacia became interested in SPR and started investigating the possibilities of the technique. In 1983, SPR sensors were introduced for the first time by Liedberg et al which was based on prism coupling [4]. Later in 1984, Pharmacia founded the company Pharmacia Biosensor AB to develop, produce and market a functional SPR-machine. The development of appropriate sensor surfaces by Pharmacia Biosensor [76-77] and the fabrication of the silicon microfluidic cartridge brought an easy-to-use SPR-machine closer to becoming a reality [16]. Over the years, different manufacturers developed other SPR systems.

Within a short period, many publications from Pharmacia Biosensor introduced the new hydrogel of dextran [77] the correlation between the SPR signal and the RIA assay [78] and gave a description of the BIACORE machine [79]. BIACORE instruments make use of a wedge-shaped laser beam and a diode array for detection, which results in no moving parts in the detection unit. The development of different, unique, more sensitive and specialized machines gave us the BIACORE X, BIACORE 2000, 3000 and Q for quality control. Other developments involved the way the liquid was handled.

In general, SPR machines use micro fluidic channels with valves to address the sample to different sensor spots. The first machine (BIACORE A100) with dynamic addressing was released in 2005[80]. The four flow channels in the micro fluidic cartridge are much wider and have five detection spots in each channel.

SPR sensor provides greater sensitivity. Thus, even a very small variation of an analyte's RI can be detected from the large peak wavelength shift. Greater sensitivity results better accuracy of detection of an unknown analyte [81]. Plasmonic(sensing) material plays a vital role in SPR sensor performance. It is used as the sensing material for the overall surface plasmon resonance phenomenon. It guides the incident light from the cladding part to the metal dielectric surface to produce the surface plasmon wave which results in surface plasmon polariton. As SPR is used for mainly sensing in the molecular level, this material needs to be very stable in nature and also fabrication of it inside the fiber need to be compatible.

In general gold, copper, silver and aluminum are used as active plasmonic materials [82]. Use of silver material results in a sharp resonance peak which increases sensing accuracy. But it is chemically unstable and highly susceptible to oxidation which reduce the sensing performance [83]. A thin coating of graphene layer can be used as a better solution but it is very complex to fabricate and cost is comparatively higher. Gold is chemically stable because it does not oxidize easily [84]. It also shows narrow resonance peak than other available materials. So far several noticeable works have been introduced to improve the performance of SPR sensor.

3.3 Literature Review

This section presents SPR related terms which includes surface plasmon wave (SPW), surface plasmon resonance (SPR), surface plasmon polariton (SPP), evanescent field

3.3.1 Surface Plasmon Wave

SPR sensors are comprised of a glass substrate and thin gold coating. Light passes through the substrate and is reflected off of the gold coating (Fig 4.2). At certain angles of incidence, a portion of the light energy couples through the gold coating creates resonant oscillation of conduction electron and resulted in a surface plasmon wave at the sample and gold surface interface.

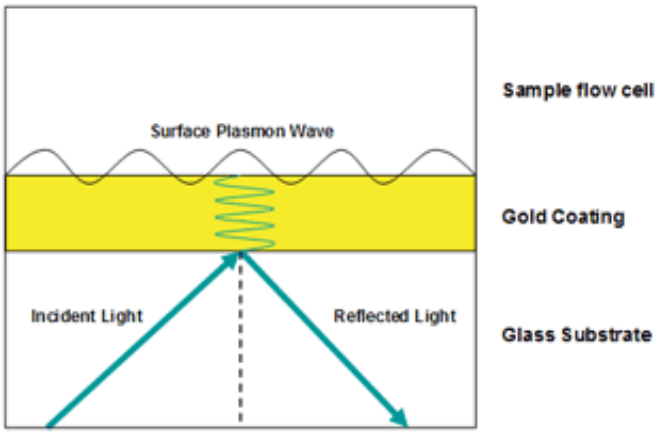

Fig 3.2 Generation of Surface Plasmon Wave

The angle of incident light required to sustain the surface plasmon wave is very sensitive to changes in refractive index at the surface (due to mass change), and also with the thickness of the layer of the sample and the gold. It is these changes that are used to monitor the association and dissociation of biomolecules. Thus, Surface plasmon wave is the main basis of surface plasmon resonance

3.3.2 Surface Plasmon Resonance

Surface plasmon resonance (SPR) refers to the excitation of surface plasmons (SPs), which are electromagnetic waves coupled on the surface between a metal and a dielectric medium (or air) propagated along the interface of the metal and dielectric material (or air) . The surface plasmon can be excited by the evanescent wave. When this happens, the intensity of the reflected light decreases sharply. The decays of the excited surface plasmon include energy conversion to photons [85].

The fundamental operating mechanism of PCF-based SPR sensors depends on the mutual interaction between evanescent field and surface electrons. The evanescent field guides the binding of the molecules which creates the SPW. In short, SPW interacts with the sensing layer due to this phenomenon. The performance of the SPR sensors depends on the geometrical parameters of the PCF.

3.3.3 Surface Plasmon Polariton

The charge motion in a surface Plasmon always creates electromagnetic fields outside (as well as inside) the metal. The total excitation, including both the charge motion and associated electromagnetic field, is surface Plasmon Polariton. They are a type of surface wave, guided along the interface in much the same way that light can be guided by an optical fiber.

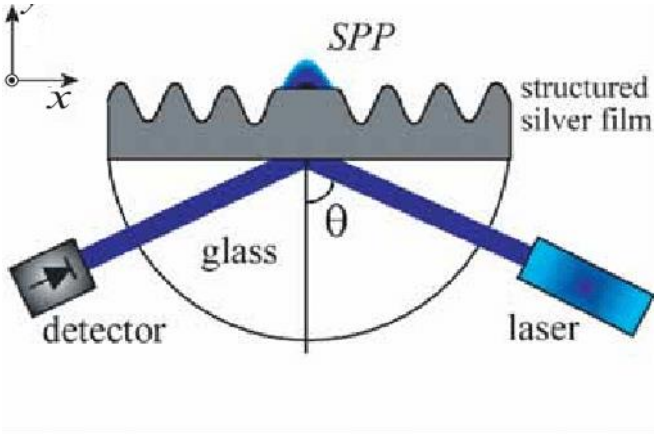

Fig 3.3 Surface Plasmon Polariton

Surface Plasmon polaritons (SPPs), are infrared or visible frequency electromagnetic waves, which travel along a metal-dielectric or metal-air interface. The term "surface Plasmon Polariton" explains that the wave involves both charge motion in the metal ("surface Plasmon") and electromagnetic waves in the air or dielectric ("Polariton"). An SPP will propagate along the interface until its energy is lost either to absorption in the metal or scattering into other directions (such as into free space) [86].

3.3.4 Evanescent Field

For light reflecting at angles near the critical angle, a significant portion of the power extends into the cladding or medium which surrounds the core. This phenomenon, known as the evanescent wave, extends only to a short distance from the interface, with power dropping exponentially with distance. The evanescent field has been exploited to allow for real-time interrogation of surface-specific recognition events [87].

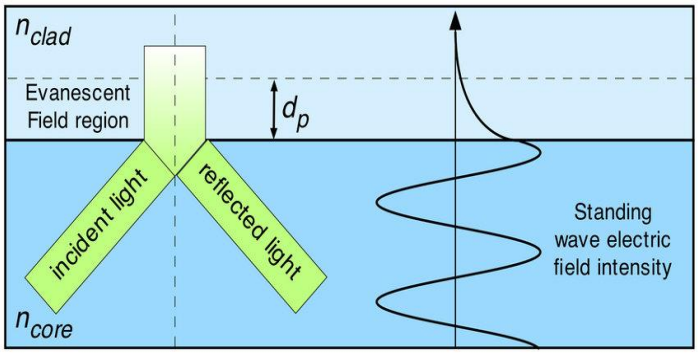

Fig 3.4 Evanescent Wave in Optical Fiber

Fiber optics are often said to use total internal reflection for guiding the light energy down the fiber, but actually a portion of the internally reflected wave extends a small distance beyond the core boundary into the optical cladding (fig 4.4).This is the evanescent wave property, which can be exploited by removing the fiber cladding to allow the evanescent wave to extend beyond the core boundary into substances surrounding the fiber core. In a system with an absorbing dielectric medium, the absorption of the medium is enhanced by the strong evanescent electric field.

3.4 Surface Plasmon Excitation by light

In order to excite SPR by irradiation with light, a phase matching condition should be satisfied which states that the excitation of SPR is possible only if the propagation constant of the light vector matches the propagation constant of the SPs [88]. According to the plasmon dispersion relation [89] for any wavelength, SPs have a longer wave vector than light waves of the same frequency propagating at the surface. This condition makes it impossible to excite SPs directly by shining incident light onto a smooth metal surface. The wave vector of light can be adjusted to match the wave vector of the SP by launching it through the metal from a medium with a RI higher than the RI of medium at the boundary where a SP is going to be excited. Standard ways to excite a SPR are to couple light through a prism [68], grating [90] or waveguide [12]. However, in recent years there has been quite an interest to excite SPR on the surface of optical fibers and sub-wavelength holes [91]. Prism coupling is one of the first tested SPR configurations and is discussed in the subsequent section.

3.4.1. Prism configuration

One of the well documented prism configurations used to excite SPR, was first reported by Kretschmann and Raether in 1968 [68]. This configuration is shown in Figure 3.5, where the setup employs a high RI prism (glass) with a metal layer on the prism's bottom and a sample on the other side of the metal layer.

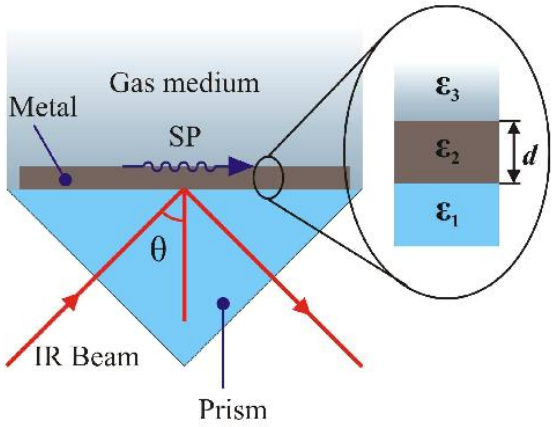

Fig 3.5 Kretschmann SPR configuration.

Light propagating in the prism is reflected at the prism-metal layer interface by means of total internal reflection. The evanescent field of the reflected light at the first interface penetrates into the metal, and if the thickness of the layer allows, it reaches the second metal-sample interface. If the RI of the second sample is smaller than the RI of the prism and also if the propagation constant of light propagating in the prism matches the propagation constant of the SP then a plasmon resonance occurs and a plasmon wave propagates at the second metal-sample interface.

3.4.2. Excitation of SPR in an optical fiber

Even though sensors currently based on the Kretschmann configuration can be relatively small, there has been an attempt to excite SPR in optical fiber to produce a more compact and reliable sensor with remote sensing capabilities. Excitation of SPR in optical fibers is similar to the excitation of SPR in the prism configuration. Light propagation in the fiber core and cladding in the form of modes experience total internal reflection at the cladding-core and cladding-exterior medium interfaces. Different modes hit the cladding-core and cladding-exterior medium interfaces

at different angles. Similarity between light propagation in the optical fiber via total internal reflection and in prism configuration have led to many successful attempts to realize SPR sensors in optical fibers.

Recently, remarkable progress has been made to SPR, localized SPR and photonic crystal fiber technologies, new types of optical fiber SPR-based sensors have attracted growing attention in the research community. Therefore, it is not possible to review all information in these areas. The details and some excellent reviews on some of the studies can be found in the references [92-95]. Some of the general SPR fiber sensors are shown in Figures 3.7(a) - (e)

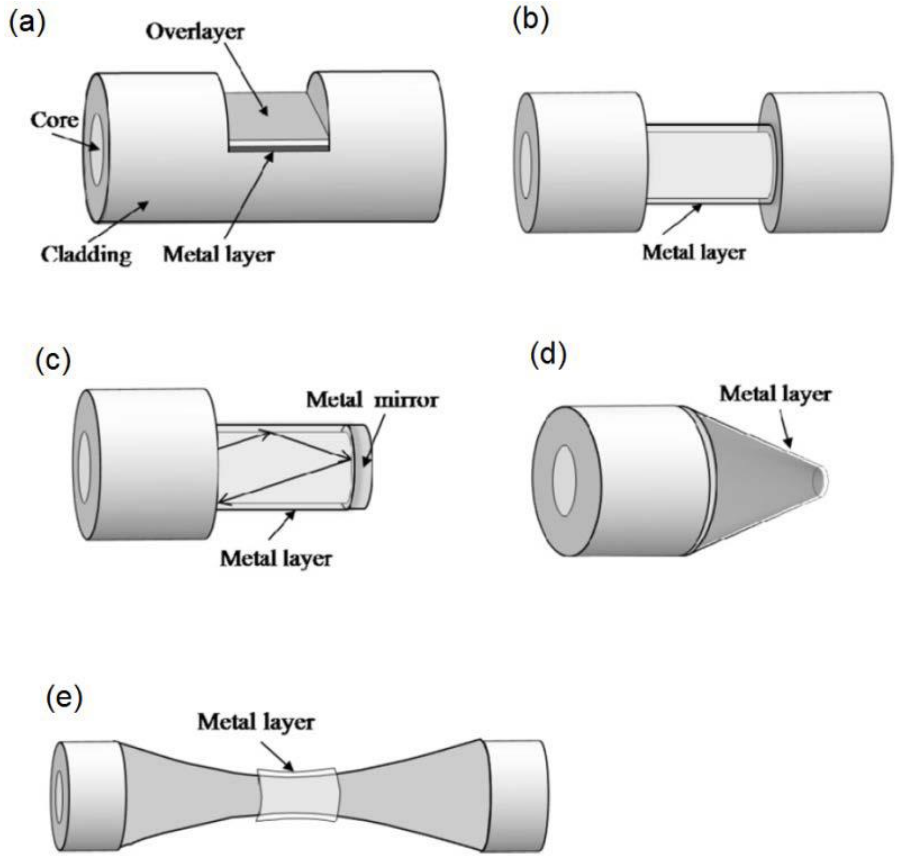

Fig 3.6 General SPR optical fiber sensors include (a) D-shape fiber, (b) cladding-off fiber, (c) end-reflection mirror, (d) angled fiber tip, and (e) tapered fiber [95].

Unfortunately, in standard telecommunications(transmission) fiber the coupling mechanism corresponding to the prism configuration is not strong enough to excite a surface plasmon resonance. If any standard fiber is coated with gold, or another SPR active metal and the phase

matching condition is satisfied by the core mode, SPR will not be excited on the fiber surface because the strength of the resulting evanescent field from total internal reflection at the core-cladding interface might be too weak to cross the cladding and interact with the metal layer. Because It is the evanescent wave which produces the primary condition for the conduction electron the metal-dielectric interface to oscillate at resonant frequency. A weak evanescent field means higher core power fraction, which results in a light unable to incident on the plasmonic layer thus no surface plasmon polariton will occur. Though Cladding modes can also be employed to excite SPR, a coupling mechanism must be provided to couple light from the core mode to cladding modes. Consequently, there are no SPR sensors based on the standard single mode fiber without deformations or modifications. Existing approaches which have been introduced so far are based on the excitation of SPR by means of enhancing the evanescent field near the metal layer and can be divided in two groups.

In the first group of approaches, the fiber is deformed in such a way that the metal layer is located in proximity to the core and core-cladding interface. The evanescent field resulting from the core mode reflection at the core-cladding interface can excite a SPR if it is strong enough to reach the metal layer. The metal layer can be located in proximity of the core-cladding interface by partially or completely removing the cladding. Typically, this can be achieved by creating a deep cut in the cladding [58] or by bending the fiber and polishing one of the fiber's sides [96-100] or by use of a non-standard fiber such as D-type optical fiber [42]. Another accepted approach is to use a tapered fiber [61]. In some approaches, it has been suggested that the plain metal coating can be replaced by nanoparticle layers [101,102], which may improve the performance of SPR fiber sensors.

In general, most of the proposed optical fiber SPR sensors based on metallic nanostructure technology do not have a proper theoretical understanding. Generally, the published experimental results were used to provide solutions for the optical fiber SPR sensors. Complications occurring during the manufacturing of sensors may result in changes to the SPR phase matching condition and possibly a widening of SPR and, as a consequence, a reduced sensitivity. The research conducted to date has shown that much has been accomplished in this field. However, more work can be done to develop new approaches and to improve the performance of the proposed sensors, in order to make them more robust and simplified.

This thesis investigates the current state of the art in the fields of surface plasmon resonance (SPR) in order to make a more reliable PCF based sensor having high sensitivity with relatively low loss.

3.5 Properties of SPR

For the optical fiber-based excitation of SPR, fused Silica (SiO_2) is used for the background material as well as the core material in general and which is also for the case of our thesis. Refractive index profile of silica is wavelength dependent resulting the use of Sellmeier equation which is defined as:

$$n^2(\lambda) = 1 + \frac{B_1\lambda^2}{\lambda^2 - C_1} + \frac{B_2\lambda^2}{\lambda^2 - C_2} + \frac{B_3\lambda^2}{\lambda^2 - C_3}; \quad (3.1)$$

where n represents the RI of silica and λ stands for the wavelength of light. Moreover, Sellmeier coefficients are B1 = 0.69616300, B2 = 0.407942600, B3 = 0.897479400, C1 = $4.67914826 \times 10^{-3}$ μm^2, C2 = $1.35120631 \times 10^{-2}$ μm^2 and C3 = 97.9340025 μm^2 [103].

Drude-Lorenz [104] model is used to get the dielectric constant of gold which is:

$$\epsilon_{Au} = \epsilon_{\infty} - \frac{{\omega_D}^2}{\omega(\omega + j\gamma D)} - \frac{\Delta\epsilon.\ \Omega_L^2}{(\omega^2 - \Omega_L^2) + j\Gamma_L\omega}; \quad (3.2)$$

ϵ_{Au} is the permittivity of gold. ϵ_{∞}=5.9673 is the permittivity at high frequency. $\omega = \frac{2\pi c}{\lambda}$ is the angular frequency, ω_D = 4227.2π THz is the plasma frequency, γD = 31.84π THz is the damping frequency, $\Delta\epsilon$=1.09 is the weighting factor, Γ_L=209.72π THz is the spectral width and Ω_L = 1300.14π THz is the oscillator strength.

3.5.1 Loss

Loss or confinement loss is a crucial guiding property in SPR sensor. It is described as the reduction resulting from the finite magnitude of the regular cladding. Confinement loss can be altered with regard to parameters such as number of layers, amount of air holes, diameter of the air hole and pitch. Calculation of the confinement loss can be done by the same equation that was mentioned earlier in the section 2.3.2

The real part of the n_{eff} of the SPP mode is highly dependent on small variation of the analyte RI. A small variation of the analyte RI results in a change in the n_{eff} which is accountable for the phase

matching towards other resonance wavelength. It turns to shift the real part of n_{eff} of the SPP mode towards higher wavelength when RI is increased. At phase matching state, when core-guided fundamental mode and the SPP mode overlap, a sharp loss peak is observed at a specific wavelength. This directs that the maximum power is transferred from the core-guided fundamental mode to the SPP mode. The loss also varies with small change in RI index. With a small increase in analyte RI results in a large shift to higher wavelength in the loss peak [103].

3.5.2 Wavelength Sensitivity

Sensitivity is the most vital performance measuring parameter for SPR. The sensitivity of a sensor can be determined using both the wavelength and amplitude interrogation technique. According to the wavelength interrogation method the WS of a sensor can be calculated by [106]

$$S_W = \frac{\partial \lambda_{peak}}{\partial n_a} \text{ [nm/RIU]} \tag{3.4}$$

where, $\partial \lambda_{peak}$ indicates the difference between two consecutive resonant wavelengths and ∂n_a indicates the difference between two neighboring n_a. So greater difference between two consecutive resonant wavelength means higher sensitivity.

3.5.3 Amplitude Sensitivity

The Amplitude interrogation method is less complex and cost effective compared to the wavelength interrogation method as it does not require the wavelength interpolation. The amplitude sensitivity of the introduced sensor can be calculated from [107]

$$S_A(\lambda)[\text{RIU}^{-1}] = -\frac{1}{\alpha(\lambda, n_a)} \frac{\partial \alpha(\lambda, n_a)}{\partial n_a}; \tag{3.5}$$

where α(λ, na) is the overall loss for a particular RI at a particular lamda and RI is equal to *na* and *∂α*(*λ, na*) is the loss difference of two loss spectra for that particular RI with its adjacent ones.

By varying the analyte RI, amplitude of loss peak changes (amplitude sensitivity). The amplitude sensitivity gradually increases with an increase in film thickness because light is confined more causing less penetration of the core mode electric field into the cladding region [108]. X-polarization usually shows a better amplitude sensitivity than y-polarization as sharper loss peak is obtained at x than y polarization.

3.5.4 Sensor resolution

Sensor resolution determines the degree of detection with analyte RI variation. The resolution of a sensor can be determined by the following [105]

$$R = \frac{\Delta n_a \Delta \lambda_{min}}{\Delta \lambda_{peak}} \tag{3.6}$$

where, R represents the sensor resolution, Δn_a represents the variation of analyte RI, $\Delta \lambda_{min}$ defines the minimum wavelength resolution, and $\Delta \lambda_{peak}$ determines the difference in resonance peak shift. Resolution means sensor indicates that the sensor has the capability to detect a tiny change of RI of the order of 10^{-6}.

3.6 Design Factors that controls the sensing performance of a SPR sensor

The sensing performance of SPR sensors vary widely in accordance with the design parameters. Thus, to get the best results optimization of different parameters are needed to find the certain value at which highest sensitivity will occur with relatively low losses. This section presents the description of such influential parameters and their effects on the sensing performance

3.6.1 Effect of plasmonic material thickness on sensing performance

The thickness of the plasmonic film thickness plays an important role on the sensing performance. It also significantly affects the resonance wavelength shift. Increasing it resulted in a reduced loss depth thickness, more than that, increasing it causes a shifting of the peak loss towards a longer wavelength. Also, higher thickness contributes to the lower entrance of the evanescent field towards the surface, causing less amplitude sensitivity. Thus, there is an inverse relation between thickness and sensitivity. If thickness is increased the excited polaritons have to travel more space to reach and interact to the analyte. Increase in thickness gradually decreases the light penetration which shifts the loss peak to a higher resonant wavelength [109].

3.6.2 Effect of cladding and core air hole diameter on sensing performance

Variation in cladding air holes affects the amplitude sensitivity. It can be seen that the variation of the diameter of the air hole from its optimum causes the loss peak to widen and reduces the amplitude sensitivity.

With increase in diameter of core air holes, causes the confinement loss to scale up. Because with larger core air hole diameter the n_{eff} difference between core and cladding gets smaller. As a result, loss increases [110].

3.6.3 Effect of pitch distance on sensing performance

By varying the pitch distances, the sensor displays no significant change in wavelength sensitivity, nevertheless significant changes in amplitude sensitivity is found. However, in some cases, resonant peak shifts to higher wavelength with decreasing pitch size and shifts to lower wavelength with increasing pitch size. Also, with increase in pitch (Λ) value, the loss peak shifts towards the shorter wavelength with increased confinement loss value because of light being confined less tightly with core region [109].

3.6.4 Effect of PML thickness on sensing performance

PML has very little impact on the confinement loss and also on the sensitivity. In case of our design which will be presented in the later chapter it was found that reduction of PML thickness below 1.0 μm resulted in a great change in amplitude sensitivity but PML thickness greater than 1.0 μm produced similar sensing performance.

3.6.5 Effect of RI of the analyte on sensing performance

RI has the most significant effect on the sensing performance of SPR sensor. Higher confinement loss, increases the field penetration through the cladding area. This suggest that maximum energy transfers from the core guided mode to SPP mode. With the rise of the analyte RI, the refractive index contrast between the core-guided mode and the SPP-mode decreases and the sensor becomes more sensitive. Increasing RI decreases the sensing length because the length of a sensor is totally dependent on the absorption loss. Thus, sensitivity peak shifts to higher resonance wavelength and broadens the overall curve with increased RI and vice versa.

Chapter 4: A review on PCF Fiber Based on Surface Plasmon Resonance

4.1 Introduction

Kretschmann and Reathers went up with a concept of a SPR detector in 1968, where direct deposition of a thin metal layer on the base of a prism coupler was demonstrated [68,111,112]. In 1983, Liedberg et al. demonstrated SPR sensor for the first-time using prism coupling for chemical and biological applications [113,114,108], however, they require many optical and mechanical (moving) components that make them bulky and unsuitable for remote sensing. To overcome these difficulties, R.C. Jorgenson first planned about optical fiber based SPR sensor in 1993, where the fiber core was coated with the gold film to reveal the plasmons response [58]. Fiber based SPR sensors are extremely useful due to its multiple attractive features such as efficiency, real-time detection, convenient operation controllable birefringence, high confinement, single mode propagation and controllable evanescent field [114-117]. The fiber based SPR sensors are widely used as they are small in size and cost effective and are used in applications such as water testing, maintain food quality, bio-sensing, medical diagnostics, gas detection, bio-imaging, environment monitoring, organic chemical sensing, real time monitoring, glucose monitoring, disease detection and so on for its high sensitivity characteristics [114,118-120,107, 110].

The plasmonic metal plays a dynamic role on the sensing performance of a SPR biosensor. At present, various types of plasmonic metals are being used such as silver, aluminum, TiO_2, copper, graphene and gold [121]. Silver would have been a perfect plasmonic metal due to its less optical damping and sharp resonance peak, however, silver has the oxidation problem which affects the sensing ability. Copper is another strong candidate to be a potential plasmonic metal. Among them, gold is the plasmonic material that is mostly used because it is chemically stable and has no problem with oxidation [122].

Two kinds of sensing systems are involved in a SPR based PCF sensor: one is internal sensing, the other is external sensing. When the analyte selectively fills the air gaps, the sensing is called internal, while the sensing process is called external sensing when the analyte is positioned on the surface of a PCF. Among the internal sensing SPR, the most recent work reported was by Rifat et

al. [123] proposing a gold coated sensor that resulted a maximum wavelength and amplitude sensitivity of 11000 nm/RIU and 1420 RIU^{-1} respectively. A number of D-shaped external sensor were reported the past couple of years. Among the reported D-shaped structures, Md. Ekhlasur Rahaman et al. in 2018 reported wavelength sensitivity of 3000 nm/RIU and amplitude sensitivity of 241 RIU^{-1} [18]. In 2015, Wang et al. reported a maximum wavelength sensitivity of 12450 nm/RIU within the RI range of 1.345–1.410 [124].

Both internal sensing approach as well as D-shaped structure of the external sensing approach consist some limitations. Among external sensors where analyte channel is in contact with the outer surface of the PCF, Liu et al. obtained a maximum wavelength sensitivity of 15180 nm/RIU within the analyte RI of 1.40 to 1.43 [125].

In 1999, Jir'ı´ Homola et al. published a review paper that summarizes development and emerging trends in SPR-sensing. Major applications were outlined where SPR sensors are used. It also said about commercialization of surface plasmon resonance sensor technology on market and future trends in development of SPR sensors [118].

We categorized different sensors according to their plasmonic materials: gold, bimetallic, silver, ITO. In gold and silver section, we further categorized according to their lattice structure and in bimetallic section we categorized them according to gold-silver, gold-TiO_2 and silver-graphene. Performance based on wavelength and amplitude interrogation method are explicitly explained. Maximum amplitude sensitivity, wavelength sensitivity and resolution are recorded for each sensor with respect to their RI range. Also, we have explained how phase matching points are varied with changing parameters like diameter, PML, thickness of gold (Au) or silver (Ag), sensing layer and pitch.

We also proposed two designs similar to the designs implemented by other researchers in order to make comparison. In the first design we proposed a gold coated circular lattice PCF based SPR sensor which showed wavelength and amplitude sensitivity of 2300 nm/RIU and 264.7 RIU^{-1}, respectively. In the second design we proposed a gold coated hexagonal lattice PCF based SPR sensor. The simulation result showed wavelength and amplitude sensitivity of 3000 nm/RIU and 459.05 RIU^{-1}, respectively.

4.2 Design Structure and Performance of PCF-SPR sensors

The SPR sensors are categorized according to its surface plasmonic material (gold, silver, bimetallic, etc.). The plasmonic metal layer can be coated inside or outside the fiber surface in a

PCF. The performance of SPR sensor highly depends on the geometrical parameter of PCF. Design parameters should be chosen carefully for a simple interaction between metal layer and evanescent field. Sensitivity is more when there is strong coupling between core guided mode and SPP mode. By optimizing different geometrical parameters of PCF based on surface plasmon resonance, we are able to get maximum wavelength sensitivity and amplitude sensitivity.

4.3 SPR sensor Using Gold Metallic Layer

Based on reported design, this section presents a detail analyzation of different kind SPR designs, their characteristics and comparison among them that used gold as the metallic layer

4.3.1 Having Hexagonal Lattice

In 2018, A. K. Paul et al. introduced a highly sensitive PCF- SPR sensor where the gold film, having thickness of t_g = 30 nm, is placed outside the PCF structure. The lattice structure has elliptical air-holes with major axis diameter d_a = 1.61 μm and minor axis diameter d_b = 0.7 μm, arranged in a hexagonal structure. The figure has been shown in Fig. 4.1(a). All elliptical air holes are well united to ensure proper coupling between the surface plasmon polariton (SPP) and the polarized mode of x or y. In both x and y polarized modes, a maximum sensitivity of 19000 nm/RIU, amplitude sensitivity of 910 RIU^{-1}, and maximum RI resolution of 5.26×10^{-6} RIU were found in the analyte refractive index (RI) range of 1.36 to 1.40. By varying the thickness of the gold film, the confinement loss and amplitude sensitivity were observed. As thickness was increased both confinement loss and amplitude sensitivity decreased and at t_g = 30 nm the sensitivity performance found was the highest. This sensor is very efficient and highly sensitive, therefore can be used for medical diagnosis and unknown detection of analytes. The sensitivity could be further improved if there are small air holes implemented between the gaps of two large air holes [106].

In 2015, A. A. Rifat introduced a hexagonal lattice PCF-SPR sensor, shown in Fig. 4.1(b), that had an active plasmonic gold layer. The analyte (sample) was put outside the fiber framework rather than inside the air-holes, resulting in a more straightforward and simple fabrication method. Two holes next to the core are removed to increase birefringence. Two air-holes in the second rings are as same size as the center air-hole to concentrate the evanescent field at two opposite sides of the fiber. The analysis stated that with an increase in RI, the resonance peak jumped to the longer

wavelength and the loss depth was simultaneously improved owing to the reduced core-cladding index. The suggested sensor showed a peak favorable sensitivity of 4000 nm/RIU and sensing resolution of 2.5×10^{-5} RIU. The loss depth also lessened due to increase in gold layer thickness. To get better signal to noise ratio, the gold t_g= 40 nm was the optimized thickness. In addition, the highest sensitivity for amplitude was 320 RIU^{-1} with a resolution of 3.125×10^{-5} RIU which are comparatively less compared to other papers and is less applicable in practical applications [110]. In another work of A. A. Rifat, in 2016, where he proposed a similar PCF-SPR sensor where the gold and sensing layer were placed outside the fiber. It had three rings of air-holes arranged hexagonally along with two smaller air-holes. In addition to the small air-holes, to excite the metal surface, two other holes were omitted to create a gap for the evanescent stream. The sensor showed the wavelength and amplitude sensitivities of 1000 nm/RIU and 118 RIU^{-1}, respectively. In addition, the suggested sensor displayed sensor resolution of 1×10^{-4} RIU and 8.5×10^{-5} RIU, with respect to the wavelength and amplitude interrogation method. The paper did not present any change in sensitivity due to change in geometrical parameters. It can only be applicable for biological and biochemical analytes detection. The figure is shown in Fig. 5.3.1(c) [126].

Table 4.1
Analysis on different properties of SPR sensors having hexagonal lattice

Reference	Sensing Approach	RI Range	Maximum Wavelength Sensitivity (nm/RIU)	Maximum Amplitude Sensitivity (RIU^{-1})	Maximum Sensor Resolution (RIU)
[106]	External	1.36–1.40	19000	910	5.26×10^{-6}
[110]	External	1.33–1.37	4000	320	3.125×10^{-5}
[126]	External	1.33–1.37	1000	118	8.5×10^{-5}

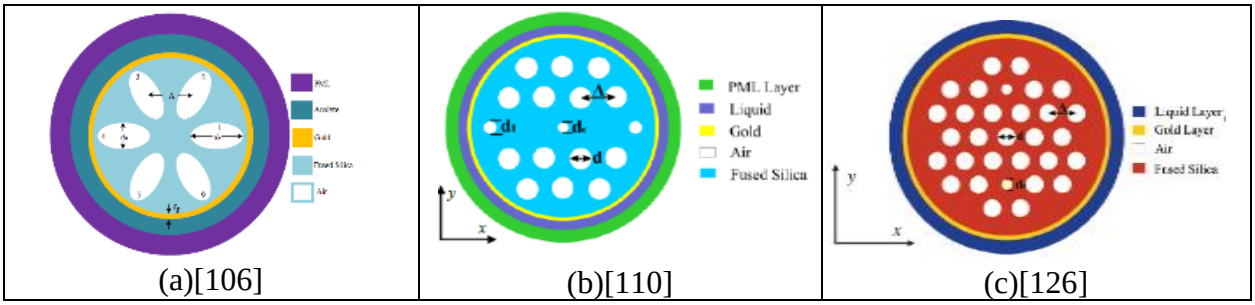

(a)[106] (b)[110] (c)[126]

Fig. 4.1. Cross sectional view of (a) hexagonal lattice PCF with elliptical air-holes, (b) hexagonal lattice PCF biosensor based on SPR, (c) simple 3 ring, hexagonal PCF biosensor based on SPR

4.3.2 Having D-shape lattice

It's really difficult to fill the analyte into the air holes and coat the metal films, therefore D-shaped PCF based SPR sensors are introduced as they are easy to fabricate and less time consuming. In 2016, Rahul Kumar Gangwar and Vinod Kumar Singh came up of a D-shaped PCF-SPR sensor. The structure is made of two layers of optical air-holes [in Fig. 4.2(a)] where diameter of first air-holes is a little smaller than the second ones. The first- and second-layer air holes have diameter d_s= 0.40 μm, d_l =0.80 μm, not only that, thickness of plasmonic gold material is kept at t_g = 0.04 μm. The confinement loss achieved were to be 79.20, 73.60, 56.55, and 49.06 dB/cm, respectively, when the RI of the analyte differed from 1.43 to 1.46. The maximum sensitivity was calculated to be 9000 nm/RIU with a very high resolution of 1.30×10^{-5} RIU. The variation of the confinement loss with different geometrical parameters were determined to improve the performance of the sensor. However, in loss versus wavelength analysis, the peak loss decreases with respect to increase in analyte RI. It also showed with an increase in pitch (Λ) value, the loss peak shifted towards the shorter wavelength with bigger confinement loss. The reason is because increase in pitch value causes less confinement of light towards the core region. When the thickness of gold (t_g) was 0.03 μm the maximum loss of 107.11 dB/cm was observed. The confinement loss of the sensor decreased as the thickness of gold [109].

A modified D-shaped PCF based surface plasmon resonance (SPR) sensor can be implemented for the detection of biological analytes, organic chemicals, bio-molecules, and other analytes. Emranul Haque et al. came up with this sensor, in 2018, which had a RI detection of analyte ranging from 1.18 to 1.36 and gold (Au) as a plasmonic material layer placed outside the D-shaped PCF structure [in Fig. 4.2(b)]. Due incomplete coupling between core mode and SPP mode it offered maximum wavelength interrogation sensitivity of 20000 nm/RIU and maximum amplitude interrogation sensitivity of 1054 RIU^{-1}. In fact, the suggested sensor displayed maximum wavelength interrogation resolutions of 5×10-6 RIU and amplitude interrogation resolutions of 16.7×10^{-6} RIU. The amplitude sensitivity and wavelength sensitivity found are relatively high compared to other D-shaped SPR sensors [127].

In 2015, Guangyao Wang et al. presented a D-shaped PCF with square-lattice having a nanoscale gold film on the flat fiber surface. All the sizes of air holes are identical with diameter d_1= 1.2 μm with a pitch value of Λ = 2 μm. By various analysis techniques, the highest wavelength and amplitude sensitivity were found to be 12,450 nm/RIU with analyte RI ranging from 1.345 to 1.41.

With increasing RI from 1.345 to 1.41 the resonance peak experienced a red shift from 745 to 1470 nm. The loss variation was implemented with respect to change in refractive index and pitch value. The sensitivity could have been further improved if the impact on loss due to variation of thickness of gold were implemented. Not only that, amplitude sensitivity was not considered in this paper. This sort of sensor is useful in fiber bio-sensing applications. The sensor is shown in Fig. 4.2(c) [124].

Table 4.2
Analysis on different properties of SPR sensors having D-shaped lattice

Reference	Sensing Approach	RI Range	Maximum Wavelength Sensitivity (nm/RIU)	Maximum Amplitude Sensitivity (RIU^{-1})	Maximum Sensor Resolution (RIU)
[109]	External (Side polished)	1.43–1.46	9000		1.30×10^{-5}
[127]	External (Side polished)	1.18–1.36	20000	1054	5×10^{-6}
[124]	External (Side polished)	1.345– 1.410	12450		

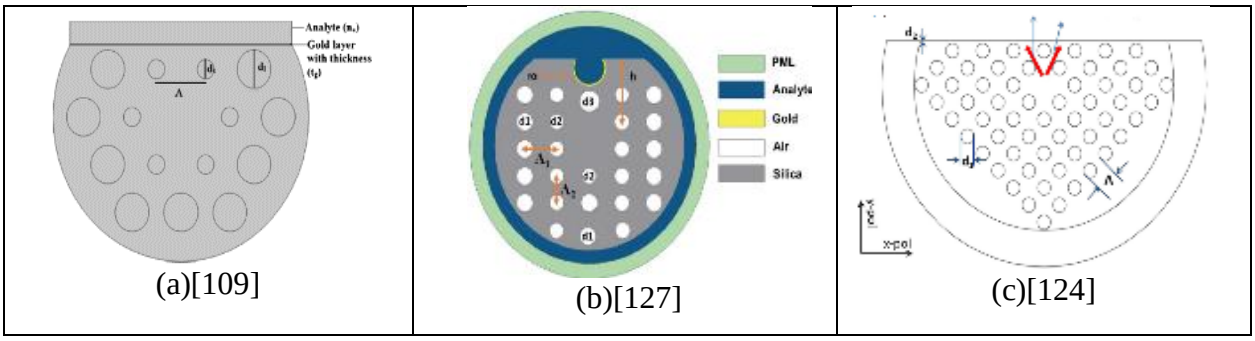

(a)[109] (b)[127] (c)[124]

Fig. 4.2. Cross sectional view of (a) D-shaped PCF with hexagonal lattice, (b) modified D-shaped PCF which has air-holes arranged in in rectangular lattice formation, (c) D-shaped PCF with square-lattice.

4.3.3 Having Circular lattice

In 2018, Shumaia Sharmin et al. introduced a simple gold-coated circular PCF-SPR sensor [in Fig. 4.3(a)] consisting of two air holes in the first ring and eight air holes in the second ring. As shown in Fig. 4.3(a) the air holes are stationed at 60-degree anticlockwise rotations with four air holes missing in the second one to create asymmetric structure. The optimum design parameters taken

are fixed at $\Lambda = 2\mu m$, $d = 0.2\ \Lambda$, $d_c = 0.3\ \Lambda$, $d_1 = 0.6\ \Lambda$, $d_2 = 0.4\ \Lambda$ and $t_g = 40$ nm to get an excellent sensing performance. The sensor showed maximum wavelength sensitivity of 8000 nm/RIU and a maximum amplitude sensitivity of 198 RIU^{-1} with a resolution of 1.25×10^{-5} RIU in the analyte RI range of between 1.33-1.39. The gold layer thickness made a significant impact not only on confinement loss but also on amplitude sensitivity. Changes in loss and amplitude sensitivity were implemented with respect to changes in pitch, gold thickness and analyte RI [116].

M. A. Mollah introduced a simple circular lattice SPR-PCF sensor which was highly sensitive and had plasmonic material (gold) of thickness $t_g = 30$ nm outside the PCF structure. The sensor consists of two rings. In the first ring, there are eight air holes with diameter d_1=1 μm while in the second ring, there are four air holes having the diameter of $d_2 = 1.6$ μm and another four having the diameter of $d_3 = 0.4$ μm. Maximum wavelength sensitivity, amplitude sensitivity, and resolution found were 12,000 nm/RIU, 2044 RIU^{-1}, 8.33×10^{-6} RIU, respectively in the analyte range of 1.37–1.41. The confinement loss decreased when film thickness was increased to observe sensor performance. The gold film thickness was optimized to 30 nm where the sensor showed the best sensing performance. The sensor is shown in Fig. 4.3(b). The sensor is highly applicable for bio-sensing applications [121].

Sensing performance is said to be high when there is high coupling between core-guiding mode and SPP mode. Md. Saiful Islam introduced an external sensing PCF-SPR sensor, as shown in Fig. 4.3(c), that had an analyte channel at the outer surface. Different air holes d, d_1 and d_2 diameters are used to form the cladding, which has an important impact on confinement loss and propagation of light through the fiber. The core shape is kept rectangular to have an asymmetric structure in order to improve birefringence. The parameters taken are listed as follows: $H = 0.5$ μm, $W = 0.15$ μm, $\Lambda = 1.8$ μm, $\Lambda_1 = 1.6$ μm, $\Lambda_2 = 1.24$ μm, $d = 1.35$ μm, $d_1 = 1.20$ μm, $d_2 = 0.18$ μm, $t_g = 30$ nm, $t_a = 0.9$ μm, and $t_p = 1.0$ μm. The author after analysis found the wavelength sensitivity of 1000, 2000, 2000, 3000, 3000, 5000, 8000, 13000, 15000, and 62000 nm/RIU respectively in the range analyte RI of 1.33 to 1.43 are. The circular and rectangular shaped air holes can be achieved using stack and draw and extrusion technique. Sensing performance could be further improved if modifications of thickness of plasmonic material is taken into consideration. This sensor is normally used in biomedicine, chemistry for accurate and precious detection of other biological and biomedical agents [128].

TABLE 4.3
Analysis on different properties SPR sensors having circular lattice

Reference	Sensing Approach	RI Range	Maximum Wavelength Sensitivity (nm/RIU)	Maximum Amplitude Sensitivity (RIU^{-1})	Maximum Sensor Resolution (RIU)
[116]	External	1.33-1.39	8000	198	1.25×10^{-5}
[121]	External	1.37–1.41	12000	2044	8.33×10^{-6}
[128]	External	1.33–1.43	62000	1415	1.61×10^{-6}

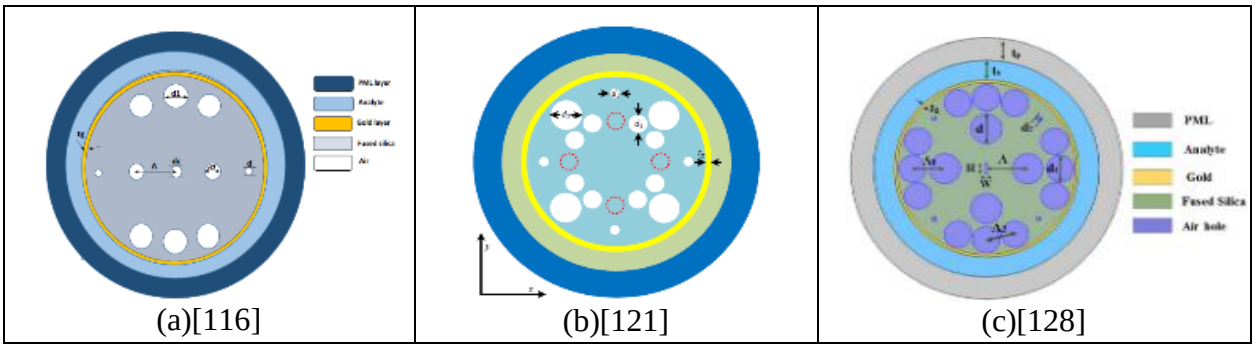

(a)[116] (b)[121] (c)[128]

Fig. 4.3. Cross sectional view of (a) a simple gold-coated circular lattice PCF based SPR sensor, (b) simple circular lattice SPR-PCF, (c) two-layer circular lattice photonic crystal fiber (PCF) biosensor.

4.3.4 Having hybrid, spiral, trapezoid lattice

In 2017, Alok Kumar Paul et al. introduced a gold-coated SPR-PCF biosensor which is shown in Fig. 4.4(a). It has a gold layer deposited at the outer surface with a thickness of 40 nm. It also has two rings of air holes. The first ring is arranged in a circular pattern and the second ring is arranged in a hexagonal pattern thus forming a hybrid lattice structure. Different analysis based on confinement loss, wavelength sensitivity, resolution was carried out by varying analyte ranges from 1.35 to 1.38. The suggested fiber had a maximum wavelength sensitivity of 4500 nm/RIU and amplitude sensitivity of 347 RIU^{-1}. It had maximum resolution of about 2.22×10^{-5} RIU and high degree of linearity of about 0.99405. The performance of the sensor highly depends on the thickness of gold film. At t_g = 40 nm, the sensor showed maximum sensitivity, thus was considered optimum gold layer thickness. This type of sensor is highly used in bio-sensing applications [129]. In 2019 Suoda Chu et al. implemented a trapezoidal (TC-PQF) six-fold PQF biosensor. The PQF-based sensor, as shown in Fig. 4.4(b), has several optical benefits due to its distinctive design, such as flattened zero-dispersion profile for a broad range of wavelength and low confinement loss,

ensuring precision and stability throughout the sensing phase. It consists of four layers of air holes of d = 1 μm with no core air hole in a six-fold PQF framework. An open trapezoid-shaped analyte channel is located at the top center of the fiber cross-section in order to infuse the analyte into the channel. The height of the trapezoid channel, d_a was 2 μm. For surface plasmon excitation, a uniform thin gold film layer of 50 nm thickness is covered at the base of the channel. The distance between top and core is d_1 = 4.5 μm. The suggested sensor demonstrated a maximum refractive index (RI) sensitivity of 4400 nm/RIU, 6100 nm/RIU, 8000 nm/RIU and 17000 nm/RIU respectively, for analytes RI range of 1.44 to 1.57, 1.41 to 1.51, 1.40 to 1.49 and 1.40 to 1.44. It was also found out that with an increase in analyte liquid height the sensitivity of the TC-PQF biosensor had increased but caused sensing range to reduce. This sensor can detect different raised RI chemicals, biochemicals and organic chemical specimens [119].

Md. Rabiul Hasan et al. introduced a SPR biosensor-based on dual-polarized spiral PCF in 2018. Chemically stable gold material is used outside the PCF structure, as shown in Fig. 4.4(c). It has a spiral cross-sectional view consisting of six arms and three rings. It should be noted that there are two air holes lacking in the first ring along the horizontal axis to generate asymmetry. The birefringence resulted in enhanced coupling between core guiding mode and SPP mode. The diameter of the central air hole is $d_c = 0.2\times\Lambda$ and remaining air holes are $d = 0.65 \times \Lambda$, while keeping Λ value to 2 μm. From y-polarized mode, the maximum wavelength sensitivity of 4600 nm/RIU and amplitude sensitivity of 420.4 RIU^{-1} were obtained and from x-polarized mode, maximum wavelength sensitivity of 4300 nm/RIU and amplitude sensitivity of 371.5 RIU^{-1} were obtained [122].

Table 4.4
Analysis on different properties of SPR sensors having hybrid, trapezoidal and spiral lattice

Reference	Sensing Approach	RI Range	Maximum Wavelength Sensitivity (nm/RIU)	Maximum Amplitude Sensitivity (RIU^{-1})	Maximum Sensor Resolution (RIU)
[129]	External	1.35–1.38	4500	347	2.22×10^{-5}
[119]	External	1.40–1.44	17000		
[122]	External	1.33–1.38	4600	420.4	2.69×10^{-5}

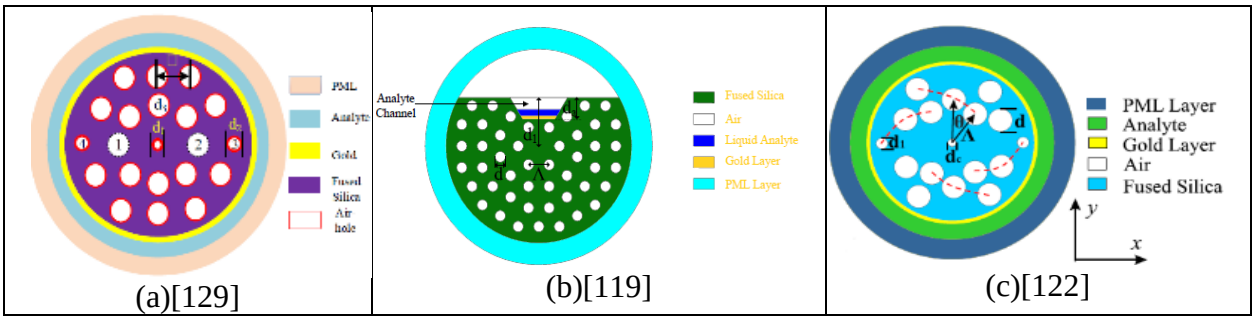

(a)[129] (b)[119] (c)[122]

Fig. 4.4. Cross sectional view of (a) a hybrid cladding structured dual core PCF based SPR sensor (b) a six-fold PQF biosensor with a trapezoidal channel (TC-PQF), (c) dual-polarized spiral PCF based biosensor.

4.3.5 Having Random Structure

As a biosensor for surface plasmon resonance, Ahasan Ullah launched a microstructured optical fiber with lens-shaped air holes [in Fig. 4.5]. It has a unique structure where tiny central air hole is surrounded by four identical biconvex lens-shaped air holes. The central hole lessened the core mode effective index which in turn caused phase matching with the plasmonic mode. By tuning radii of lens shaped air holes (r_1) and the distance between the intersecting points (l) resonance wavelength, modal confinement loss and sensitivity of the sensor could be controlled and analyzed. Simulation result showed a maximum amplitude sensitivity of 500 RIU^{-1}, a maximum wavelength sensitivity of 5000 nm/RIU and a resolution of 2×10^{-5} RIU [112].

Table 4.5
Analysis on different properties on SPR sensor having random lattice structure

Reference	Sensing Approach	RI Range	Maximum Wavelength Sensitivity (nm/RIU)	Maximum Amplitude Sensitivity (RIU^{-1})	Maximum Sensor Resolution (RIU)
[112]	External	1.33–1.345	5000	500	2×10^{-5}

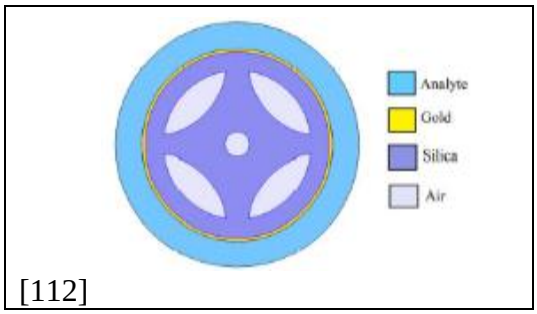

[112]

Fig. 4.5. Cross-sectional view of SPR biosensor based on microstructured fiber with lens shaped air holes.

4.3.6 Structural Design and simulation of a reported design

We implemented a previously reported PCF-SPR with external sensing approach circular lattice in Fig. 4.6 using finite element method (FEM)-based COMSOL 5.3a software. This sensor is similar to the sensor suggested by Md. Saiful Islam et al. in [130]. The plasmonic material that we used here is gold. The reported sensor has circular lattice structure with 2 rings of air-holes. There are two air-holes missing in the second layer in order to create birefringence. In the second ring air-holes are arranged in 30° anticlockwise progressive rotation while in the first ring air-holes are arranged 60° anticlockwise progressive rotation. Three air-holes are made smaller than the rest in order to accumulate evanescent field at two opposite sides of the PCF. The parameter taken are: pitch distance Λ= 2 µm, diameter of smaller air holes $d_1 = 0.2\Lambda$ µm, diameter of bigger air-holes d= 0.4Λ µm, thickness of the gold film t_g= 40 nm.

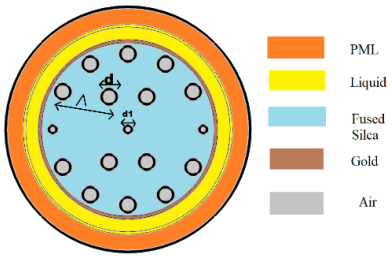

Fig. 4.6. Cross-sectional view of the reported circular lattice PCF sensor with $d_1 = 0.2\Lambda$ µm, d= 0.4Λ µm, Λ= 2 µm and t_g= 40 nm.

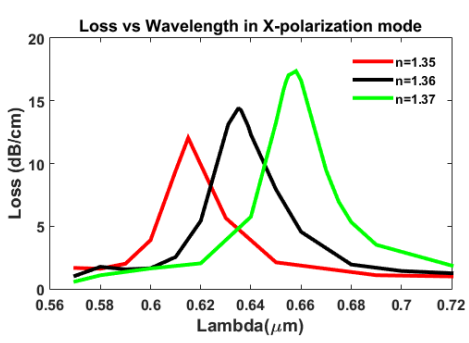

(a)

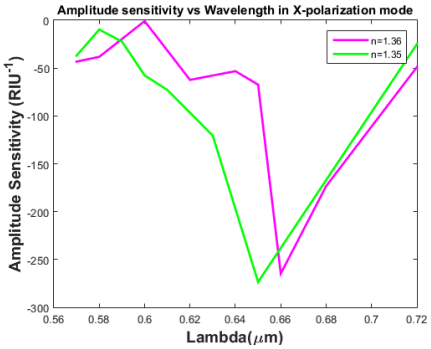

(b)

Fig. 4.7 (a) Fundamental loss variation for increasing analyte RI from 1.35 to 1.37, (b) amplitude sensitivity for different analyte RI with $d_1 = 0.2\Lambda$ μm, $d = 0.4\Lambda$ μm, $\Lambda = 2$ μm and $t_g = 40$ nm.

A small change in analyte RI causes the phase matching point to shift. Fig. 4.7(a) shows that higher analyte shifts the resonance wavelength shift towards a higher wavelength. Increasing the analyte's RI leads to a reduction of the index contrast between the core and cladding, thus causing an increase in confinement loss. The lowest confinement loss of 12.03 dB/cm was found for an analyte RI of 1.35 and highest loss of 17.03 was observed at analyte RI 1.37 at 0.655 um wavelength. By using wavelength interrogation and amplitude interrogation method the sensitivity of the proposed sensor can be analyzed. From Fig. 4.7(b), amplitude sensitivity of 62.347 RIU^{-1}, 53.208 RIU^{-1}, 67.275 RIU^{-1} are found at 0.6200 μm, 0.6400 μm and 0.6500 μm, respectively. The reported sensor shows maximum wavelength sensitivity of 2200 nm/ RIU and maximum amplitude sensitivity of 261 RIU^{-1} at RI of 1.36.

4.4 SPR sensors using Bimetallic Materials

To enhance the evanescent field, many researchers used bimetallic layer instead of one single gold outside the cladding surface and at certain conditions obtained better result than using only gold as the metal layer which is presented in brief in this section

4.4.1 Using Gold+ TiO_2

To overcome adhesion problem of gold a thin TiO_2 layer with elevated RI with non-toxicity and environmental compatibility characteristics is frequently used between Au and glass. Recently, in June 2019, Saiful Islam et al. published a paper where they introduced simple, miniature, and highly SPR-PCF biosensor. A 30-nm thick gold (Au) layer supported the surface plasmons whereas thin titanium dioxide (TiO_2) layer was used to assist adhesion of gold on the glass fiber. The fiber cross-section, as shown in Fig. 4.8(a), is created by circular-shaped holes that simplified the process of preform production. Also, using an array of air holes in the middle of the fiber, a high-birefringence was acquired. The performance analysis of the proposed sensor was carried out by optimizing different geometrical parameters that included Au film thickness t_g, TiO_2 film thickness t_t, air hold diameters d and d_1, and a number of core air holes n_c. The authors carried out the analysis by varying the geometrical parameters that included gold thickness t_g, number of air holes in core n_c, air hole diameters d and d_1 and thickness of TiO_2. The following parameters are

used as optimum for sensing performance: $d_c = 0.125\Lambda$, $d = 0.67\Lambda$, $d_1 = 0{:}09\Lambda$, $\Lambda = 1.65$ µm, $\Lambda_1 = 1.16$ µm, $n_c = 5$, $t_g = 30$ nm, and $t_t = 5$ nm. From this sensor the maximum wavelength sensitivity 25,000 nm/RIU, maximum amplitude sensitivity 1,411 RIU^{-1} were recorded [115].

There are always opportunities to create a low cost SPR biosensor. Md. Saiful Islam et al. introduced a localized surface plasmon resonance (LSPR) that could combine both wave-guiding and plasmonic resonance sensing. LSPR is an optical phenomenon that is a result of surface plasmon excitation in nanoparticles or nanograting's of a size smaller than the wavelength of light. $D_c = 0.18\Lambda$, $d = 0.70\Lambda$, $d_1 = 0.09\Lambda$, $\Lambda = 3.75$ µm, $t_a = 1.5$ µm, and $t_p = 1.80$ µm are taken as optimum parameters as shown in Fig. 5.4.1(b). The sensor showed a maximum wavelength sensitivity of 111000 nm/RIU and high amplitude sensitivity of 2050 RIU^{-1}. It also showed a high resolution of 9×10^{-7}. It also had the capability to detect any analyte within a refractive range from 1.33 to 1.43 in the visible to mid-IR. The LSPR showed a sharper loss peak in around 1.85 times larger AS than with SPR. Not only that, LSPR requires less Au and TiO_2, which increases cost-effectiveness for real-world applications. The thickness of both Au and TiO_2 were varied to find the best possible sensitivity of the optical sensor. Scientists are now focusing on LSPR since it showed very high performance compared to previous sensors [131].

Table 4.6
Analysis on different SPR sensors having gold and TiO2 as plasmonic layer

Reference	Sensing Approach	RI Range	Maximum Wavelength Sensitivity (nm/RIU)	Maximum Amplitude Sensitivity (RIU^{-1})	Maximum Sensor Resolution (RIU)
[115]	External	1.33–1.38	25 000	1411	4×10^{-6}
[131]	External(dual side polished)	1.33–1.43	111000	2050	9×10^{-7}

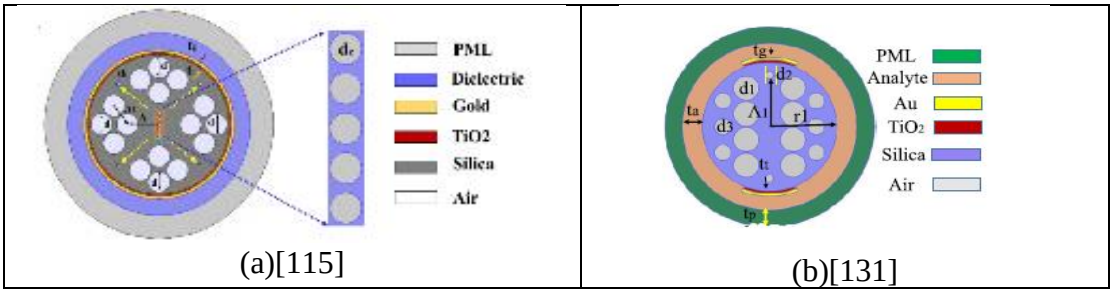

(a)[115] (b)[131]

Fig. 4.8 Cross-sectional view of (a) a hi-bi ultra-sensitive surface plasmon resonance fiber sensor, (b) a localized surface plasmon resonance (LSPR).

4.4.2 Using Silver+ Graphene

Ahmmed A. Rifat et al. introduced a PCF-SPR sensor with selectively filled analyte channels. Silver is used as plasmonic material to detect analytes correctly and is covered with a slender coating of graphene to avoid oxidation [in Fig. 4.9]. The liquid-filled cores are positioned close to the metal channel. The lattice is triangular in structure and value of pitch and air-hole diameter are $\Lambda = 1.90$ μm, $d = 0.5\Lambda$, respectively. On the other hand, the analyte core diameter and the metallic channel diameter are equal, $d_1 = d_c = 0.8\ \Lambda$. The silver and graphene thicknesses are set as $t_g = 35$ nm and $t_g = 3$ nm, respectively. Performance analysis was measured with respect to analyte RI, thickness of silver, liquid-filled air-hole diameter. The maximum wavelength sensitivity calculated was 3000 nm/RIU. Also, the maximum amplitude sensitivity was 410 RIU^{-1} with a high resolution of 2.4×10^{-5} RIU [108].

Table 4.7
Analysis on different properties of SPR sensor having graphene and silver as plasmonic layer

Reference	Sensing Approach	RI Range	Maximum Wavelength Sensitivity (nm/RIU)	Maximum Amplitude Sensitivity (RIU^{-1})	Maximum Sensor Resolution (RIU)
[108]	Internal (selective coating)	1.46–1.49	3000	410	2.4×10^{-5}

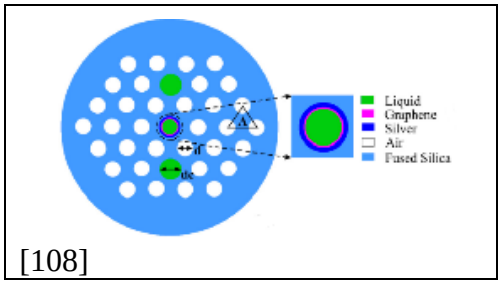

[108]

Fig. 4.9 Cross-sectional view of SPR sensor with selective analyte channels and graphene-silver deposited core.

4.4.3 Using Gold+ Silver

An SPR-PCF biosensor having two metalized microfluidic slots constructed by gold and silver as plasmonic material was launched by Akowah et al. back in 2012 [shown in Fig. 4.10]. Gold is deposited at the top of the silver to assist as protection against oxidation and other chemicals. As shown in fig. 8, some air holes in the second ring are made smaller for effective phase matching between core guided mode and surface plasmon modes. The second ring has two uniform thickness slots that surrounded the analyte. Parameter values taken are: Λ=1.5 μm, d_1/Λ=0.5, d_{01}/Λ =0.22, t_{Au}=5 nm, t_{Ag}=45 nm. The sensor was able to get a low sensitivity of 3200 nm/RIU which was its highest wavelength sensitivity. Due to large micro-fluidic slots, the structure is relatively easy to fabricate [132].

Table 4.8
Analysis on different properties of SPR sensor having gold and silver as plasmonic layer

Reference	Sensing Approach	RI Range	Maximum Wavelength Sensitivity (nm/RIU)	Maximum Amplitude Sensitivity (RIU^{-1})	Maximum Sensor Resolution (RIU)
[132]	External		3200		

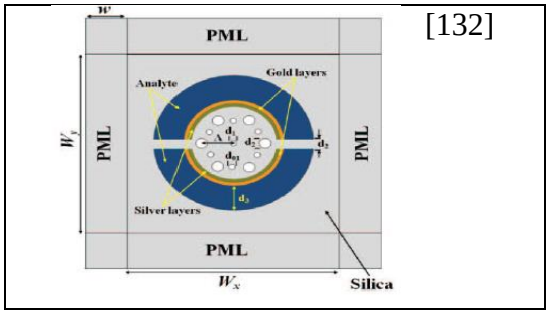

[132]

Fig. 4.10 Cross-sectional view of PCF-SPR sensor based on bimetallic structure of gold and silver.

4.4.4 Structural Design and analysis of another reported design

Similarly, we implemented another photonic crystal fiber (PCF) sensor based on surface plasmon resonance design as shown in Fig. 4.11 The design is similar to the design implemented by Rajan Jha [133] which had graphene layer on silver coated PCF. But in our proposed design we used only gold as plasmonic material to compare the sensitivity and loss between the two designs. Using Comsol Multiphysics 5.3a software simulation is carried out.

The sensor has a central hole that is surrounded by six holes arranged in a hexagonal manner. The holes are separated by a distance Λ= 2 µm. There are six air holes both at top and bottom. The second layer consists small air holes used as fine confinement of light in a particular direction. Larger holes lead to confinement of light towards the core. According to the fig. 14, the parameters taken are: d_2= 0.2 Λ, d_b= 0.4Λ, d_c=0.3Λ, d_1=0.6Λ. The thickness of gold used is 40 nm.

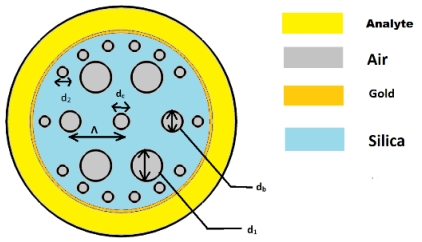

Fig. 4.11 Reported PCF based SPR sensor having a hexagonal lattice structure with Λ= 2 µm, d_2= 0.2 Λ, d_b= 0.4Λ, d_c=0.3Λ, d_1=0.6Λ.

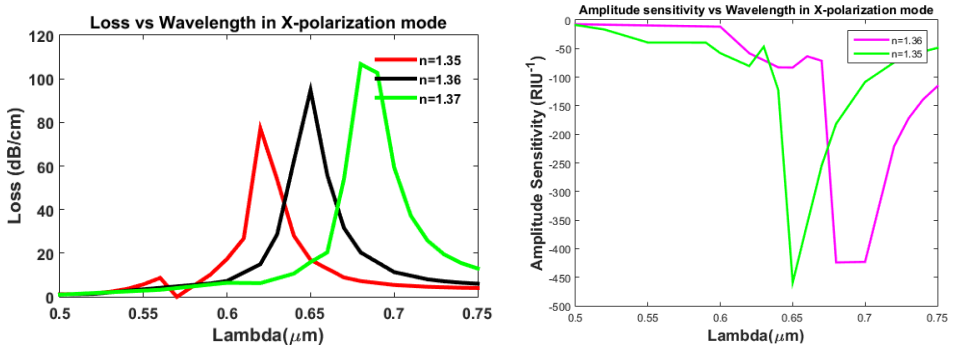

(a) (b)

Fig. 4.12 (a) Fundamental loss variation for increasing analyte RI from 1.35 to 1.37, (b) amplitude sensitivity for different analyte RI with Λ= 2 µm, d_2= 0.2 Λ, d_b= 0.4Λ, d_c=0.3Λ, d_1=0.6Λ.

From Fig. 4.12 (a) we see peak losses at 0.62 µm, 0.65 µm and 0.68 µm at three different analyte RI in x-polarization mode. Loss of 77.18 dB/cm, 94.79 dB/cm and 106.69 dB/cm are found in analyte RI 1.35, 1.36 and 1.37, respectively. We also see that phase matching between core mode and SPP mode shifts to higher resonant wavelength.

Furthermore, the performance of the sensor is evaluated by the mean of amplitude and wavelength sensitivity. As shown in Fig. 4.12 (b), the maximum amplitude sensitivity of 459.05 RIU^{-1} is

obtained at 650 nm wavelength for the analyte RI n_a= 1.35. The maximum wavelength sensitivity calculated is 3000 nm/RIU.

By using gold as plasmonic material the sensitivity of this sensor increased drastically than the design at [133], provided all the parameters are kept constant. The design shown in [133] provided maximum amplitude sensitivity of 860 RIU^{-1} and a maximum loss of 600 dB/cm at 1.37. The wavelength sensitivity has not been calculated in that paper. It also did not show the x- and y-polarization of the PCF. The performance of the sensor also could be improved if we varied the thickness of gold, diameter of air-hole. The performance could also be improved by adding a PML.

4.5 SPR Sensor Using ITO

The permittivity of ITO is modeled using [11]:

$$\varepsilon(\omega) = \varepsilon - \frac{\omega_p^2}{\omega^2 + i\omega\Gamma} \tag{4.1}$$

where ε = intra-band dielectric constant, Γ= damping coefficient, $\omega_p^2 = ne^2/\mu\varepsilon_0$, $\mu = 0.3m_e$, m_e = free electron mass, ω_p = 2.19ev and Γ= 0.111ev.

The refractive index profile can be obtained from the following equation [116],

$$n_t = \sqrt{5.913 + \frac{2.441 \times 10^7}{\lambda^2 - 0.803 \times 10^7}} \tag{4.2}$$

where, n_t denotes the RI of TiO_2 and λ is in Angstroms.

Thin film TiO_2 raises the surface plasmon excitation which in turn increases the evanescent field. It also has high refractive index than the fiber and whenever placed on the glass creates strong coupling between the core guided and the plasmonic mode, thus enhances sensing performance [115].

Using indium tin oxide (ITO), the plasmonic resonance can be adjusted by altering the inherent characteristics of the materials by altering the number of metal atoms and oxygen content. Jitendra Narayan Dash and Rajan Jha, in 2014, introduced a SPR sensor based on conducting metal oxide (ITO) that guided surface plasmon wave at the interface of dielectric and ITO. By changing the thickness of ITO, one could tune the peak resonant frequency but unlike other plasmonic materials, no band to band transitions were involved in case of ITO. Moreover, ITO is more economic that gold and silver, thus cost-effective. As shown in Fig. 4.13(a) parameters of the sensor taken Λ = 2μm, d_1/Λ = 0.5, d_2/Λ = 0.8, d_3/Λ = 0.65, d_c/Λ = 0.4, t = 70 nm, where t is the thickness of the ITO

layer. The sensor managed to show a high sensitivity of 2000 nm/RIU. Using amplitude and wavelength interrogation method the resolution achieved were 12×10^{-5} RIU and 5×10^{-5}, respectively [117].

Two years later, the same authors introduced a similar SPR sensor based on ITO but was given d-shape in structure. A commonly recognized etching or edge polishing method can achieve the necessary d-shaped framework. As shown in Fig. 4.13(b), along x-direction, the diameter of the core is 4.3 μm. There are two large holes which has diameter 4.5 μm and the smaller holes has diameter of 2.2 μm, while keeping pitch value of 4.4 μm. Thickness of ITO were varied to survey of shifting of resonant wavelength. Also, wavelength sensitivity were calculated with variation of analyte RI from 1.330 to 1.350. The maximum sensitivity was found 17000 nm/RIU along with a resolution of 5.8×10^{-6} RIU which is higher than previous sensor using ITO [134].

Table 4.9
Analysis on different properties of SPR sensors having ITO as plasmonic layer

Reference	Sensing Approach	RI Range	Maximum Wavelength Sensitivity (nm/RIU)	Maximum Amplitude Sensitivity (RIU^{-1})	Maximum Sensor Resolution (RIU)
[117]	Internal (multi-coating)		2000	80	5×10^{-5}
[134]	External (side polished)	1.330– 1.350	17000	74	5.8×10^{-6}

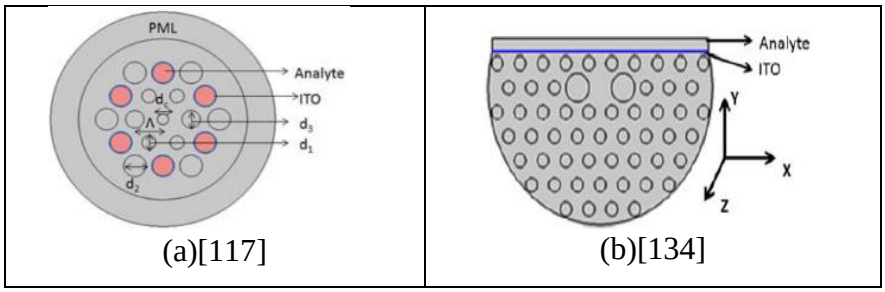

(a)[117] (b)[134]

Fig. 4.13 Cross-sectional view of (a) SPR biosensor based on conducting metal oxide (ITO), (b) SPR sensor based on a side-polished birefringent PCF coated with ITO

4.6 SPR Sensor Using Silver

The relative permittivity of silver (ε_{Ag}) is obtained by [32]:

$$\varepsilon_{Ag}(\omega) = \varepsilon_{\infty} + \frac{\sigma/\varepsilon_0}{i\omega} + \sum_{p=1}^{4} \frac{C_p}{\omega^2 + A_p i\omega + B_p}; \quad (4.3)$$

where, ε_{∞}= intraband dielectric constant at infinity, ω= resonant frequency, ε_{Ag} = permittivity of silver.

4.6.1 Having D-shaped structure

Chao Liu et al. presented a symmetrical dual parallel D-shape PCF-SPR sensor that is highly used in the area of chemistry, biomedicine, and integrated optics. In Fig. 5.6.1 silver layers are coated on the vertical planes and have a thickness of t_{Ag} = 50 nm. As seen in the figure, parameters taken are r_a = 100 nm, d = 900 nm, and r = 12 um where r_a represents the radius of the air holes, d represents distance between two fibers and r represents the distance between the air hole array in an arc-shape and center of a single fiber. $\Lambda_1 = 2r\sin(\pi/16)$ represents distance between adjacent air holes in an arc shape whereas $\Lambda_2 = 2r / 4$ is the distance between vertically arranged adjacent air holes. By simulation, the results obtained were 1222 RIU^{-1} which was the maximum amplitude sensitivity and 14660 nm/RIU which was the maximum wavelength sensitivity when the analyte refractive indexes are varied from 1.39 to 1.40. Also, the average sensitivity reached were 14660 nm/RIU with a sensing resolution of 6.82×10^{-6} RIU [135].

Table 4.10
Analysis on different properties of SPR sensor having D-shaped structure

Reference	Sensing Approach	RI Range	Maximum Wavelength Sensitivity (nm/RIU)	Maximum Amplitude Sensitivity (RIU^{-1})	Maximum Sensor Resolution (RIU)
[135]	Internal (dual side polished)	1.36–1.41	14660	1222	6.82×10^{-6}

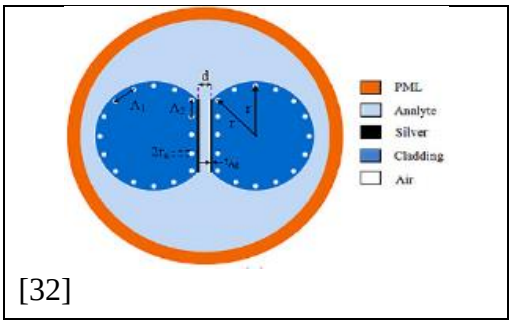

[32]

Fig. 4.14 Cross-sectional view of symmetrical dual D-shape PCF-SPR sensor

4.6.2 Having Circular Shaped lattice

A hollow-core PCF SPR sensor with circular lattice air holes was proposed by authors Moriom Rojy Momota and Md. Rabiul Hasan in 2017. In the exterior surface of the PCF framework, [shown in Fig. 4.15] a slim coating of silver is used. The second circle contained two air-hole rings with four missing air holes. The air holes in the second ring were larger than the first ring for better light containment in the desired direction. In order to obtain high sensing performance, they used the following design parameters Λ = 2 mm, d = 0.57Λ, d_1= 0.78 Λ and t_s = 30 nm. The sensor displayed a maximum wavelength sensitivity of 4200 nm/RIU with a wavelength resolution of 2.38×10^{-5} RIU. The maximum amplitude sensitivity of 300 RIU^{-1} with a high wavelength resolution of 3.33×10^{-5} RIU is also obtained for an analyte refractive index of 1.37. The length of the sensor can be expanded to centimeters due to small confinement loss [120].

Table 4.11
Analysis on different properties of SPR sensor having circular shaped lattice

Reference	Sensing Approach	RI Range	Maximum Wavelength Sensitivity (nm/RIU)	Maximum Amplitude Sensitivity (RIU^{-1})	Maximum Sensor Resolution (RIU)
[120]	External	1.33–1.37	4200	300	3.33×10^{-5}

[120]

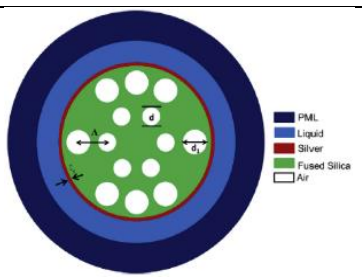

Fig. 4.15. Geometrical cross-sectional view of a hollow-core PCF SPR sensor.

4.7 Discussion

From the last few decades, researchers have tried to improve the performance of PCF based SPR sensors by developing distinct structures within the sensors. They have carried out different progresses in order to gain maximum sensitivity with low confinement loss and improved performance. Having structural simplicity and good sensing performance made its usefulness in biomolecules and chemical analyte detection.

By reviewing the papers from 2010 to 2019 on PCF based on surface plasmon resonance, we can get an idea of what type of sensors and geometrical parameters provide higher sensitivity or loss depth. Fused silica is used almost every SPR sensors as background material since it has ultra-low thermal sensitivity. Perfectly matched layer (PML) added at the outer layer potentially absorbs radiation energy. Although PCF-SPR sensors provide higher sensitivity that transmission-based PCF they are often difficult to fabricate. External sensing approach PCF-SPR sensors provide higher amplitude sensitivity and wavelength sensitivity than internal sensing approach sensors. Circular lattice genuinely creates more improved sensitivity than hexagonal and trapezoid lattice structures because more of light confinement. Multiple small air holes in a lattice means more confinement of light towards the core whereas larger air holes provoke transfer of energy from core to surface mode to increase. Moreover, pitch distance should be low otherwise there will be a large amount of leakage of light towards the cladding region. D-shaped PCF SPR sensors, where one side of PCF is polished and a metal layer applied on the flat top, also provide high sensitivity but needs precise polishing to extract portion of the PCF, which is practically challenging. Overall, it would be very difficult to fabricate irregular PCF structures that requires various sizes of holes to be placed in precise positions.

Gold is used in most of the SPR-PCF sensors as the plasmonic material as it is chemically inert, biocompatible, and can be applied easily using chemical vapor deposition method. On the other hand, bimetallic layer PCF based SPR sensor are more effective than single layer sensor. Addition of TiO_2 with gold in SPR-PCF sensors provide higher sensitivity than other bimetallic PCF sensors. Since TiO_2 has a high RI and acts as a transition metal, creates a strong evanescent wave and causes strong coupling of core mode and SPP mode, which in turn escalates sensitivity. Gold-silver based SPR-PCF sensor is not effective at all because of poor adhesion between gold and silver. Single film layer such as silver or copper are rarely used in PCF sensors since they are subjected to high oxidation problem, thus provide poor sensing performance; even though copper

is cheaper compared to gold and silver. To prevent this oxidation, graphene is coated on the metal layer as it is mechanically strong and chemically inert.

LSPR sensor has attracted a number of researchers lately due to its high sensitivity and low confinement loss. It also has gold as plasmonic metal in contact with TiO_2. It provided a maximum wavelength sensitivity of 111000 nm/refractive index unit (RIU) and amplitude sensitivity of 2050 RIU^{-1} within RI range of 1.33–1.43. It can be used for applications such as biomolecular and bio analyte detection. Nowadays, sensors showing maximum amplitude sensitivity more than 1000 RIU^{-1} are taken into account for research purposes. PCF SPR still needs a lot of improvement but it is by far a successful and affordable technology for sensing. Most of the implementation done are simulation based, it still needs to be implemented practically to be used in applications. Therefore, the performances of PCF SPR sensors are still in question. Scientists are shifting to this current technology since it has vast scope of doing researches.

Chapter 5: Simulation and Experimental Analysis of Our Proposed Design

5.1 Introduction

Surface Plasmon Resonance has become a phenomenon in the recent research works. Various types of sensing and detection is done using this technology. Richie et al. first introduced surface plasmon resonance theoretically [136]. Using this idea Otto reported the Otto configuration (1968). Liedberg et al. demonstrated SPR sensor for the first-time using prism coupling for chemical and biological applications [113]. For using prism coupling technique effectively, light has to be incident in a certain angle which is difficult. Prism using has its fair share of drawbacks such as bulky in size, limited optimization and commercialization, isn't applicable for remote sensing applications [84,133].

In 1993 R.C. Jorgenson proposed about PCF based SPR sensors. PCFs has numerous advantages over prism such as small size and design flexibility, optimization of structural parameters, optimization of core clad diameter or position, propagation of light in single mode, light launching at zero incident angle into the core etc. For these advantages it is possible to control the evanescent field and core guided leaky mode propagation, also exciting SPs are possible, very sharp resonance peak is shown in single mode PCFs and this enhances the detection accuracy [137-139].

SPR is used in sensing applications for various purposes. In medical field SPR sensors are used for DNA sensing, virus detection, miRNA detection, E. coli detection, antibiotics detection [140-149]. In chemical and alcohol sensing, SPR sensors are used for TNT, copper, ethanol, methanol, uric acid, toluene, furfural, Benz thorium detection [150-156]. Gases such as NO_2 detection is also done [157,158]. SPR sensors are also used for water and food safety purposes, environmental monitoring, industrial applications, pesticide detection, Raman and Fluorescence Spectroscopy etc. [159-165].

Silver (Ag) and gold (Au) are mostly used as plasmonic materials around the PCF structure. The resonance peak using silver is sharper than gold. So, that is why usage of silver gives the most amplitude sensitivity. But due to humidity silver gets oxidized which reduces the analyte detection

accuracy which is a great problem. That is why gold is the most popular metal to use. It is stable, bio-compatible and the resonance peak is also large enough [166].

In this paper, a circular lattice PCF is proposed where comparison between elliptical, circular, rectangular airholes are done. Gold is used as the plasmonic material. A thin layer of TiO_2 is added before gold layer because Ti enhances film adhesion capability and chemical stability and that's why better amplitude sensitivity is achieved [166].

5.2 Structural Design and Numerical Analysis

Fig 5.1(a) (b) (c) represents cross sectional view of the proposed design with circular, elliptical and rectangular airholes. They have 5 layers of airholes. Layer 1,3,5 have the same type of airholes and layer 2 and 3 have same type of airholes. D_a is the diameter for layer 1,5 circular airholes. D_b is the diameter for circular airholes of layer 2 and 4. D_c is the diameter of the center circular airhole where $D_c=D_a$.

For elliptical airholes, L_a and L_b is the a and b semi axis length for layer 1,5 respectively and L_c, L_d are the a and b semi axis length for layer 2 and 4 airholes respectively. L_{ca} and L_{cb} are the a and b semi axis length for the center elliptical airhole respectively where $L_{ca}=L_a$ and $L_{cb}=L_b$.

W_a and H_a is the width and height of the layer 1,5 rectangular airholes respectively and W_b, H_b are the width and height for the layer 2 and 4 rectangular airholes respectively. W_c and H_c are the width and height of the center rectangular airhole where $W_c=W_a$ and $H_c=H_a$.

Fused sillica is used as the background material. T_g =40nm and T_t=10nm are the thickness of the gold layer and the TiO_2 layer for all three designs. T_a is the thickness of the analyte layer.

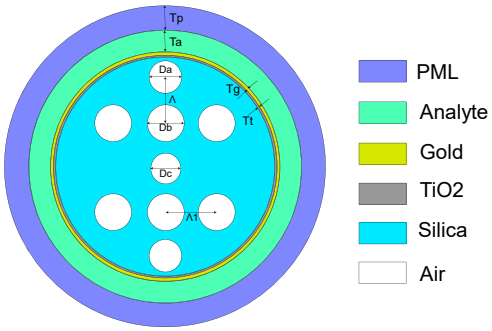

(a)

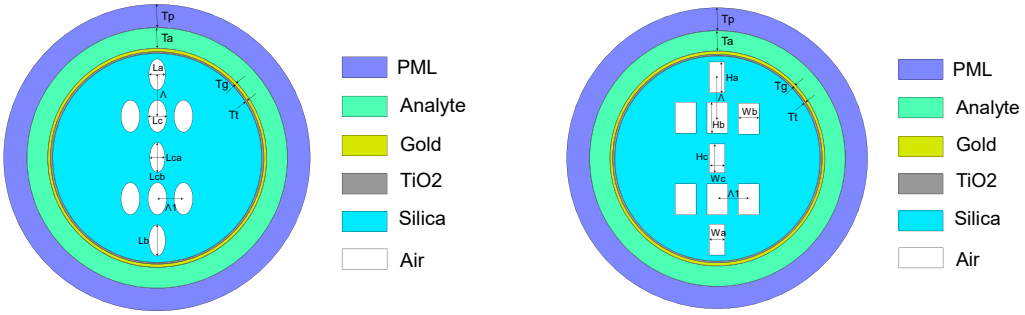

(b) (c)

Fig 5.1: Cross section of the three designs (circular, elliptical, rectangular airholes respectively)

(For circular airhole design, $D_a = D_c = 0.4\mu m$, $D_b = 0.5\mu m$, $\Lambda = 2\mu m$, $\Lambda 1 = 1.5\mu m$. For elliptical airhole design, $L_a = L_{ca} = 0.4\mu m$, $L_b = L_{cb} = 0.8\mu m$, $L_c = 0.5\mu m$, $\Lambda = 2\mu m$, $\Lambda 1 = 1.5\mu m$. For rectangular airhole design, $H_a = H_c = 0.8\mu m$, $W_a = W_c = 1.6\mu m$, $H_b = 0.5\mu m$, $W_b = 1.6\mu m$, $\Lambda = 2um$, $\Lambda 1 = 1.5\mu m$)

The refractive index of fused silica is obtained by using Sellmeier equation [167].

$$n^2(\boldsymbol{\lambda}) = 1 + \frac{B_1\lambda^2}{\lambda^2 - C_1} + \frac{B_2\lambda^2}{\lambda^2 - C_2} + \frac{B_3\lambda^2}{\lambda^2 - C_3} \tag{5.1}$$

Here n is the refractive index of fused silica and it is dependent on the wavelength($\boldsymbol{\lambda}$) which is in μm. B_1=0.69616300, B_2= 0.407942600, B_3= 0.897479400, C_1= 0.00467914826, C_2= 0.0135120631, C_3= 97.9340025 are the Sellmeier constants for fused silica.

Drude-Lorenz [104] model is used to get the dielectric constant of gold which is

$$\epsilon_{Au} = \epsilon_{\infty} - \frac{{\omega_D}^2}{\omega(\omega + j\gamma D)} - \frac{\Delta\epsilon.\ \Omega_L^2}{(\omega^2 - \Omega_L^2) + j\Gamma_L\omega} \tag{5.2}$$

ϵ_{Au} is the permittivity of gold. ϵ_{∞}=5.9673 is the permittivity at high frequency. $\omega = \frac{2\pi c}{\lambda}$ is the angular frequency, ω_D = 4227.2π THz is the plasma frequency, γD = 31.84π THz is the damping frequency, $\Delta\epsilon$=1.09 is the weighting factor, Γ_L=209.72π THz is the spectral width and Ω_L = 1300.14π THz is the oscillator strength.

5.3 Analysis of Using Circular, Elliptical and Rectangular Air holes

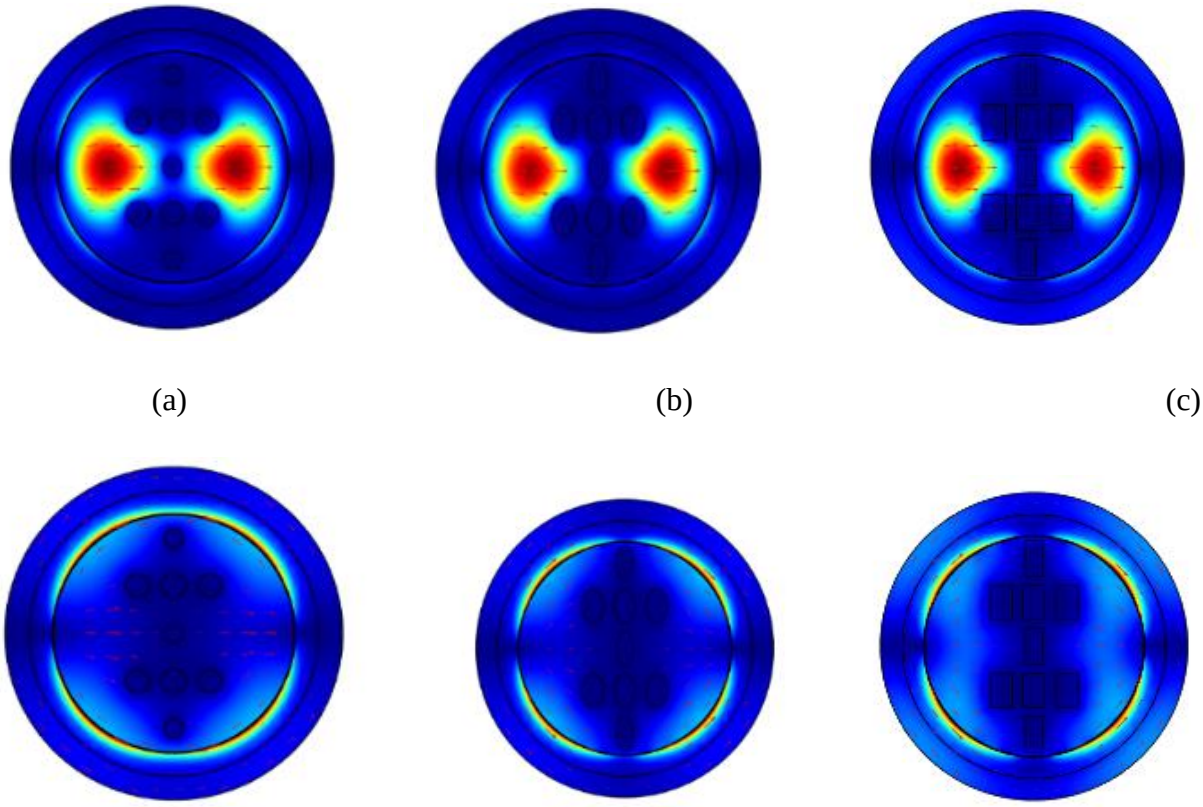

(a) (b) (c)

(d) (e) (f)

Fig 5.2: (a), (b), (c) core mode (x polarization) and (d), (e), (f) SPP mode for elliptical, circular and rectangular airholes respectively at 1.4,1.4,1.4 RI and 0.85,0.85,0.9 μm wavelength.

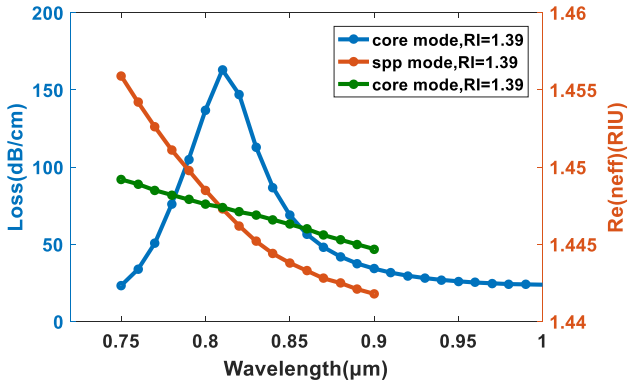

Fig 5.3: Dispersion relation between core guided mode and SPP mode

Investigation was done for both x and y polarization initially. But as x polarization gave better results than y-polarization, x-polarization was chosen for further investigation.Confinement Loss (CL) is a key parameter for the investigation of the performance of the proposed PCF. CL is calculated by the equation mentioned in section 2.3.1

Wavelength sensitivity (WS) is another important parameter to determine the sensor performance which is determined by the following equation [168]

$$S_\lambda = \frac{\Delta\lambda_{peak}}{\Delta n_a} \text{ nm/RIU} \tag{5.3}$$

Where $\Delta\lambda_{peak}$= the difference between two adjacent peak loss wavelengths for two adjacent RI, Δn_a = the difference between those two adjacent RI.

For elliptical airholes at 1.39-1.40 RI λ_{peak} are 810nm and 950nm, so WS for 1.39 RI is 14,000nm/RIU.

A very high sensor resolution is also a good indicator for great sensor performance which is calculated by the following equation [124]

$$R = \frac{\Delta n_a \times \Delta\lambda_{min}}{\Delta\lambda_{peak}} \text{ RIU} \tag{5.4}$$

For elliptical airholes $\Delta n_a = 0.01, \Delta\lambda_{min} = 0.1$ and $\Delta\lambda_{peak}$ = 140nm at 1.39-1.40 RI gives a high sensor resoluton of 7.14×10^{-6} RIU

Wavelength interrogation or phase detection method is used to determine the wavelength sensitivity. This method is cost effective but measuring process of sensitivity is very complex. To overcome this problem amplitude interrogation method is used which determines amplitude sensitivity at a fixed wavelength. Amplitude sensitivity is determined by the following equation [83]

$$S_A(\lambda) = -\frac{1}{\alpha(\lambda,n_a)}\frac{\partial\alpha(\lambda,n_a)}{\partial n_a} \text{ RIU}^{-1}$$

here, $\alpha(\lambda, n_a)$ = overall propagation loss at a specific refractive index (RI) and $\partial\alpha(\lambda, n_a)$ = difference between the two loss spectra.

All these parameters were determined for the performance analysis of the proposed design in order to ensure a better performance of the design.

5.3.1 CL and AS variation for different RI of Analyte of Circular Air holes

Same design was implemented using circular, elliptical and rectangular airholes. A 10nm of TiO_2 layer, 40 nm of gold layer and 0.96μm of analyte layer was chosen for the comparison. The highest CL, WS and AS for circular design are 177 dB/cm and -684.75 RIU^{-1} and 11,000 nm/RIU respectively (Fig 5.4: (a), (b)).

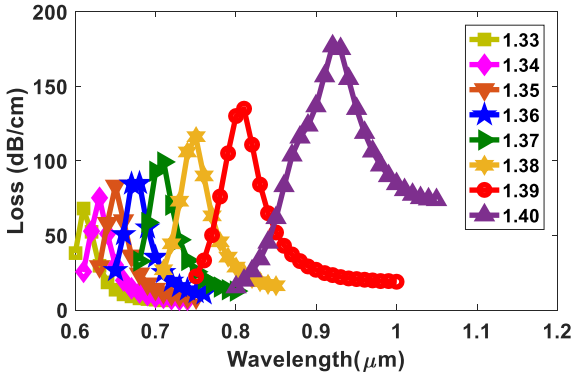

(a)

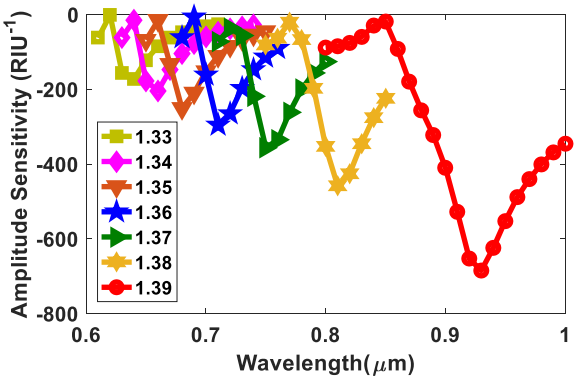

(b)

Fig 5.4: (a), (b) CL and AS variation for different refractive index of analyte for circular airholes respectively.

5.3.2 CL and AS variation for different RI of Analyte of Elliptical Air holes

For elliptical design highest CL, WS and AS are 294 dB/cm and -1,026.44 RIU^{-1}, 14,000 nm/RIU respectively (Fig 5.4: (c), (d)).

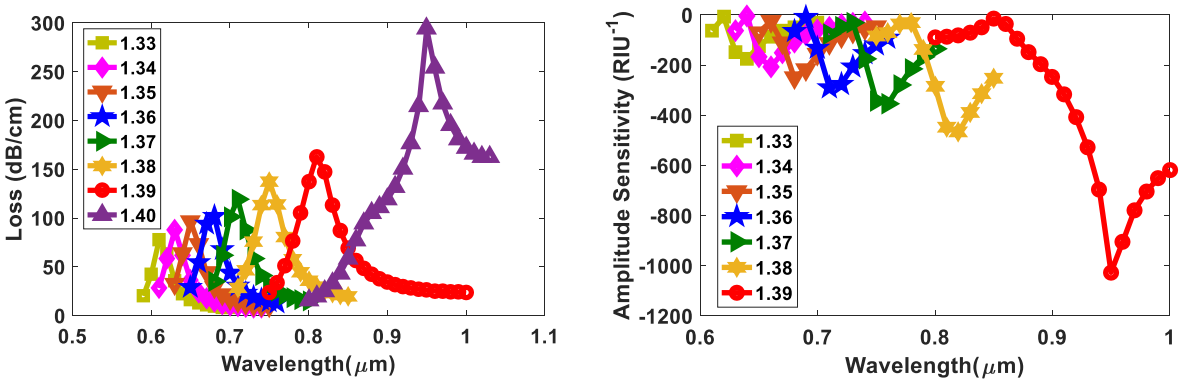

(c) (d)

Fig 5.4: (c), (d) CL and AS variation for different refractive index of analyte for elliptical airholes respectively.

5.3.3 CL and AS variation for different RI of Analyte of Rectangular Air holes

CL, WS and AS are 171.14 dB/cm, -517.83 RIU^{-1}, 16,000 nm/RIU respectively (Fig 5.4: (e), (f)) for rectangular design.

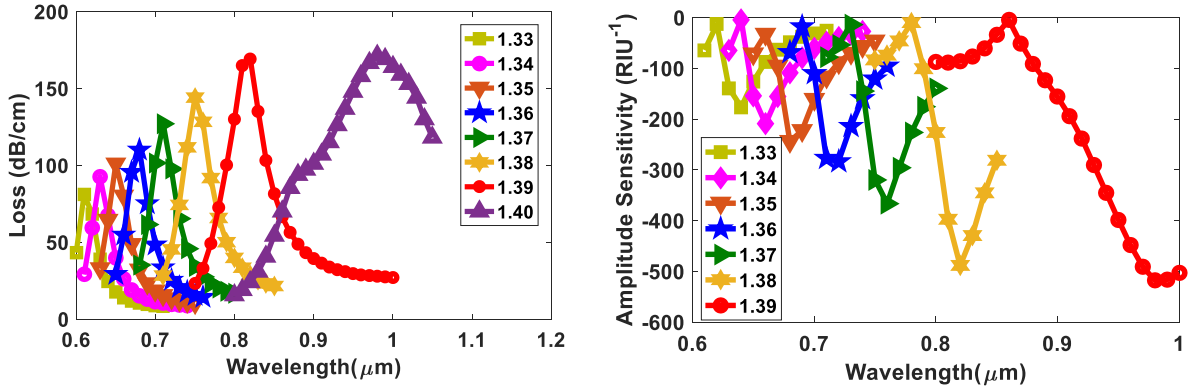

(e) (f)

Fig 5.4: (e), (f) CL and AS variation for different refractive index of analyte for rectangular airholes.

5.3.4 Comparison and Discussion

Although rectangular design has the lowest CL of 171dB/cm and highest WS of 16,000 nm/RIU, its AS is the lowest (-517.83 RIU^{-1}) among the 3 designs. Circular design has more AS (-684.75 RIU^{-1}) than rectangular design but CL is slightly more (177dB) and WS is less (11,000 nm/RIU^{-1}). From elliptical design we got the best AS of -1,026.44 RIU^{-1} and better WS (14,000 nm/RIU) than circular design but the CL was more in this case (294 dB/cm). As the AS and WS for the elliptical design is better compared to other designs which are the main parameters elliptical airholes design was selected for further investigation.

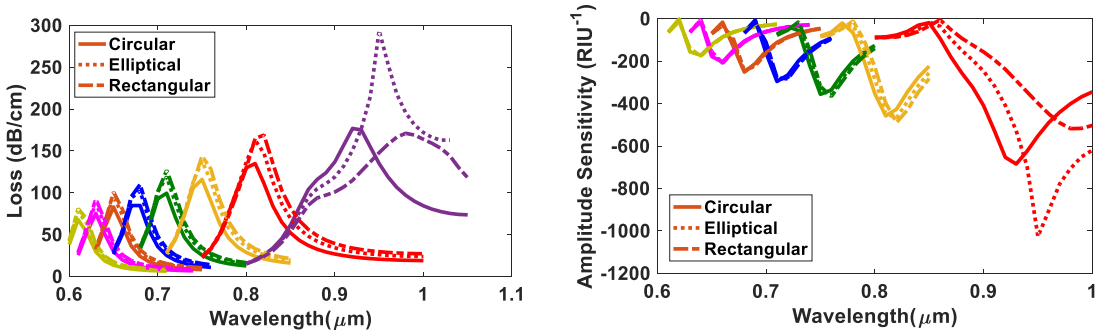

(a) (b)

Fig 5.5: (a), (b) CL and AS comparison for different types (circular, elliptical, rectangular) air holes

5.4 Optimization of Proposed Design

To achieve the best, result the proposed design is optimized in terms of the thickness of gold layer, analyte layer, TiO2 layer, PML layer and semi axis length of center airhole

5.4.1 By varying Gold layer

At first the thickness of the gold layer was considered as 30nm. For 30nm layer the highest CL and AS was 399dB/cm and -747.16 RIU^{-1} respectively. Then for 35nm CL and AS were 308.05 dB/cm and -851.27 RIU^{-1}. These results were better than 30nm ones. Then for 40 nm CL and AS were 294dB/cm and -1,026.44 RIU^{-1}. Then for 45nm thickness CL and AS were 151.57 dB/cm and -656.59 RIU^{-1} respectively where CL was less than 40nm CL, but AS was much less than 40nm AS. That's why 40nm was chosen for the optimized gold thickness for our design.

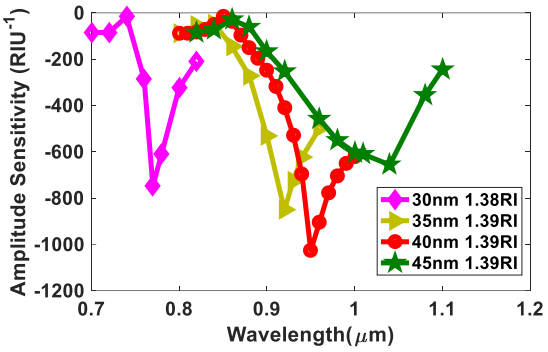

Fig 5.6: amplitude sensitivity comparison for different gold thickness (Tg)

5.4.2 By varying TiO_2 thickness

For investigating the optimized TiO_2 layer thickness at first CL and AS was taken without a TiO_2 layer which were 326.18 dB/cm and -858.55 RIU^{-1} respectively. Then investigation was done using a thin layer of 5nm which gave CL and AS of 320.24dB/cm and -993.08 RIU^{-1}. As the results improved, layer was made to 10nm and CL and AS were 294dB/cm and -1,026.44 RIU^{-1}. Again, both CL and AS improved. But adding a 15nm TiO_2 layer CL and as were 219.6dB/cm and -856.67 RIU^{-1} respectively. CL improved but AS was less than the previous one. That's why 10nm was taken as the optimum thickness (T_t) for TiO_2 layer.

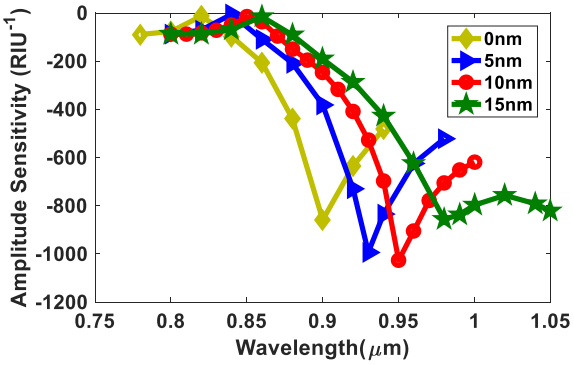

Fig 5.7: Comparison of AS for different TiO_2 thickness (T_t)

5.4.3 By varying Analyte layer Thickness

To optimize analyte layer thickness 0.9μm,0.93μm,0.96μm and 0.99μm was considered. For T_a=0.9μm, CL and AS were 159dB/cm and -495 RIU^{-1} respectively. For 0.93μm CL and AS were 232dB/cm and -817 RIU^{-1} respectively. As AS improved, T_a was increased to 0.96μm and CL and AS for that thickness were 294dB/cm and -1,026.44 RIU^{-1}. Then for 0.99μm thickness CL and AS were 252dB/cm and -865.52 RIU^{-1}. As AS started to decrease at 0.99μm thickness, 0.96μm was selected as the optimum T_a.

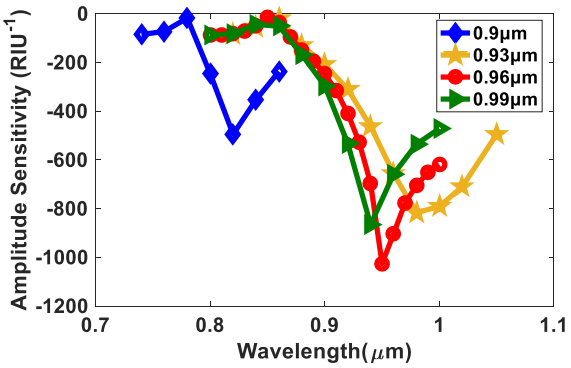

Fig 5.8: AS comparison for different T_a

5.4.4 By varying PML layer Thickness

PML optimizing was done by varying T_p from 0.94μm to 1μm. For T_p= 0.94μm, CL and AS were 244.19dB/cm and -823.68 RIU^{-1} respectively. Then for T_p=0.97μm, CL and AS were 249.86dB/cm and -836.11 RIU^{-1} respectively. AS increased with the increase of T_p. That's why T_p was increased to 1μm and CL and AS were 294dB/cm and -1,026.44 RIU^{-1} respectively. AS increased again. For T_p=1.03μm CL and AS were 244.2dB/cm and -882.12 RIU^{-1} respectively. As for T_p=1.03μm AS decreased, T_p=1μm was selected as the optimum PML thickness (T_p).

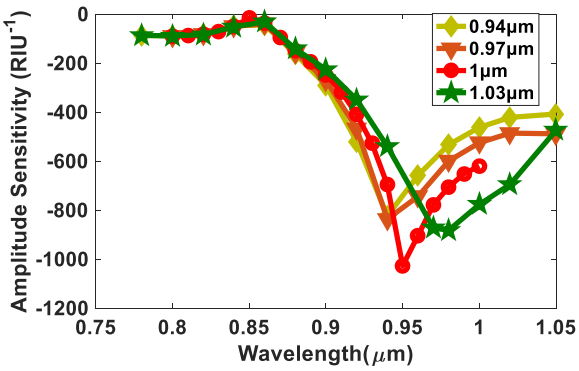

Fig 5.9: AS comparison for different T_p

5.4.5 By varying semi axis length of center airhole

Center elliptical airhole a-semi axis length was varied to optimize. For a-semi axis length of 0.2μm CL and AS was 256.7dB/cm and -925.15 RIU^{-1}. For a-semis length of 0.3μm CL and AS were 288.37dB/cm and -1028 RIU^{-1} respectively. AS increased. For a-semi axis length of 0.4μm CL and AS were 294dB/cm and -1,026.44 RIU^{-1}. AS decreased a bit. That's why 0.3μm was taken as the optimized a-semiaxis length of the center airhole.

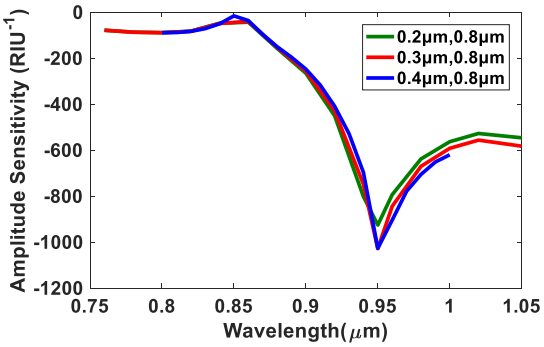

Fig 5.10: AS comparison for different a-semi axis length of center airhole

5.5 Fully optimized sensor design with metal grating

After the full optimization of the proposed design, metal grating was added instead of metal layer which then increased CL from 294dB/cm to 340dB/cm and also increased AS from 1028 RIU^{-1} to -1,189.46 RIU^{-1}.

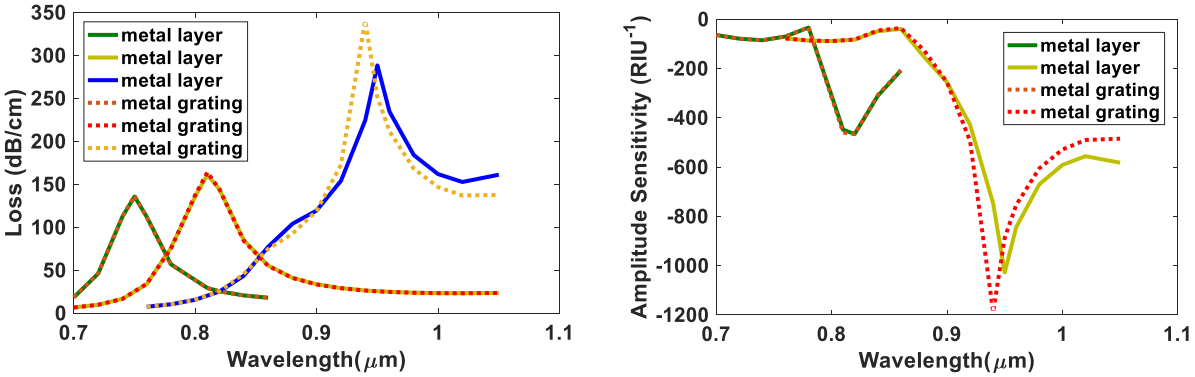

(a) (b)

Fig 5.11: (a) confinement loss variation for metal layer and metal grating

(b)AS variation for metal layer and metal grating

5.6 Linearity of the design

The linearity of the proposed sensor was also checked. Fig 11 shows the linear fitting of then resonance wavelength as a function of analyte RI. Regression equation of the linear line is y=7646.34x – 9787.68 where y= Resonance Wavelength and x= Refractive Index (RIU). R^2 value of the linear fitting curve is 0.9656 which shows better linearity.

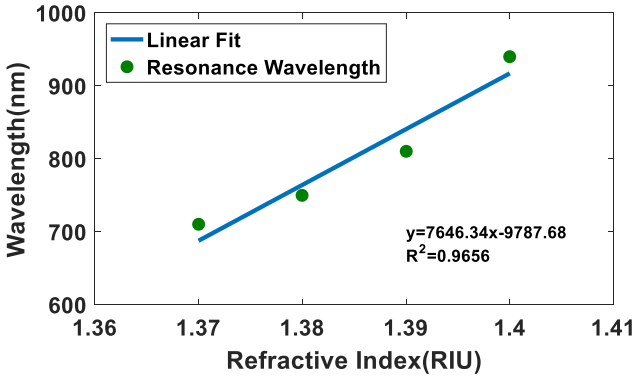

Fig 5.12: Regression line of the resonance wavelength as a function of analyte RI

5.7 Comparison with other designs

The proposed PCF is compared with other different PCF performances in Table 5.1

Table 5.1

Ref	Sensing Approach	RI Range	Amplitude sensitivity (RIU^{-1})	Wavelength sensitivity (nm/RIU)	Resolution (Amp.) (RIU^{-1})	Resolution (Wave.) (RIU^{-1})	Loss Peak (dB/cm)
[114]	External	1.34-1.37	318	9,000	N/A	1.11×10^{-5}	700.05
[169]	External	1.33-1.38	1,411	25,000	N/A	$4x10^{-6}$	N/A
[170]	External	1.36-1.39	442.11	6,000	N/A	1.66×10^{-5}	449.91
[120]	External	1.33-1.37	300	4,200	$3.33\ x10^{-5}$	$2.38\ x\ 10^{-5}$	3.061
[125]	External	1.40-1.43	498	15,180	N/A	5.6818×10^{-6}	N/A
[171]	External	1.32-1.41	1,170	34,000	N/A	$2.94x10^{-6}$	0.79
[172]	External	1.33-1.38	420.4	4,600	N/A	$2.17x10^{-5}$	4.048
[173]	External	1.33-1.40	1,085	9,000	N/A	$1.11x10^{-5}$	535
[174]	External (side Polished)	1.33-1.36	241	3,000	N/A	$3.341x10^{-6}$	18
[175]	Internal	1.4-1.44	1,739.26	9,600	$5.75x10^{-6}$	$1.04x10^{-5}$	N/A
This paper	External	1.33-1.40	1,189.46	13,000	$8.41x10^{-6}$	$7.69x10^{-6}$	340

5.8 Discussion

A circular shaped SPR based PCF is proposed with 9 elliptical airholes. As the number of airholes are minimum, fabrication will be easier. Gold and Tio2 is used as the plasmonic materials. The proposed PCF shows maximum amplitude sensitivity and wavelength sensitivity of 1,189 RIU^{-1} and 13,000nm/RIU respectively. It exhibits sensor resolution of $7.69x10^{-6}$. Besides the value of R^2 is 0.9656 which exhibits high linearity. Considering high performance of the proposed PCF, it is a good candidate for biomolecular, biochemical and biological analyte detection.

Chapter 6: Conclusion and Future Plan

6.1 Conclusion

In conclusion we can say that we have worked on two review papers (transmission, SPR) where we compared previous works based on their EML, Birefringence, Sensitivity and Confinement Loss. For transmission related review paper, the main comparing parameters were EML, Confinement Loss and Birefringence. But as for SPR related review paper the main parameters were Confinement Loss and Amplitude Sensitivity. Working on those papers, we gained the knowledge necessary to write our own design and paper. We also made our own design which is described in chapter 6 in detail. Through this design we were able to get very good results (AS of 1189.46 RIU^{-1} and CL of 340dB/cm) which helped us in deep study of Surface Plasmon Resonance and Photonic Crystal Fiber. Although we did our utmost to make the most of our time, we couldn't do all the the studies perfectly. That's why we have selected some future goals for this research work which were described previously. This thesis work helped us to be acquainted with SPR and PCF and their characteristics, how they work, principles which in turn will help us in future research works.

6.2 Socio-Economic Impact

Although fabrication of this type of PCF is not done in our country, but if it was done here this research work would have been very fruitful. This research work shows high sensitivity sensor with minimum loss which can be used to

(i) Detect plasma, blood, blood components from an unknown sample which will be very impactful in the medical research.

(ii) Determine the presence of harmful gases such as H_2S from a complex mixture which can open new fields in the chemical research field.

(iii) As AS is higher and CL is low and the design is also a simple one, it will not be very costly to fabricate than other designs out there. This will help others to realize to create new simple designs and continue the research work in PCF based SPR sensors.

6.3 Future Work

In this design we have used gold as plasmonic material and compared between circular, elliptical, rectangular airholes. We also used Tio2 for better adhesion of gold. We used silica as the background material. Although we did a tremendous job investigating the sensor performance, we couldn't do some work due to time and other technical constraints. However, in future in order to investigate further we will do the following.

(i) We will use different plasmonic materials such as silver, graphene to search for better sensitivity and better results.

(ii) Although three types of airholes are compared, there are other types of airholes which may give better results, these will be tested in future.

(iii) Same design can be implemented on D-shaped PCF to investigate the sensor performance.

(iv) We did most of our research work based on X-polarization only as this gave better sensitivity. In future Y-polarization will be explored for better comparison of the sensitivity.

(v) The sensing approach of our design was external. We will also try to arrange internal sensing approach for the same design in search for better results.

6.4 References

[1] Homola, J., Surface Resonance Sensors for Detection of Chemical and Biological Species. Chem. Rev., 108(2): p. 462-493, 2008.

[2] Homola, J., Present and future of surface plasmon resonance biosensors. Analytical and Bioanalytical Chemistry, 377(3): p. 528-539, 2003.

[3] Rich, R.L. and D.G. Myszka, Survey of the year 2005 commercial optical biosensor literature. Journal of Molecular Recognition, 19(6): p. 478-534, 2006.

[4] Leidberg, B., et al., Surface Plasmon Resonance for Gas-Detection and Biosensing. Sensors and Actuators, 4(2): p. 299-304, 1983.

[5] Homola, J., et al., Spectral surface plasmon biosensor for detection of staphylococcal enterotoxin B in milk. International Journal of Food Microbiology, 75(1-2): p.61-69, 2002.

[6] Blobe, G.C., et al., Mechanisms of disease: Role of transforming growth factor beta in human disease. New England Journal of Medicine, 342(18): p.1350-1358, 2000.

[7] Adamczyk, M., et al., Application of surface plasmon resonance toward studies of low-molecular-weight antigen-antibody binding interactions. Methods-a Companion to Methods in Enzymology, 20(3): p. 319-328, 2000.

[8] Dostalek, J., et al., Rich information format surface plasmon resonance biosensor based on array of diffraction gratings. Sensors and Actuators B-Chemical, 107(1): p. 154-161, 2005.

[9] Islam, M. R., Arif Hossain, M., Ali, S. I., Sultana, J., & Saiful Islam, M., Design and Characterization of an Ultra-Low Loss, Dispersion-Flattened Slotted Photonic Crystal Fiber for Terahertz Application. Journal of Optical Communications, 0(0). doi:10.1515/joc-2018-0152

[10] J. A. Buck, "Fundamentals of Optical Fibers," John Wiley and Sons Inc., USA, 2nd Edition, 2004.

[11] K. Kaneshima, Y. Namihira, N. Zou, H. Higa, and Y. Nagata, "Numerical investigation of octagonal photonic crystal fibers with strong confinement field," IEICE Transactions on Electronics, vol. E89-C, no. 6, pp. 830-837, 2006.

[12] Y. Hibino and H. Hanafusa, "Formation mechanism of drawing induced peroxy radicals in pure silica optical fibers," J. Appl. Phys. Vol. 62, pp. 1433, 1987.

[13] B. Liedberg et al "Biosensing with surface plasmon resonance – how it all started." Biosens.Bioelectron. 10: i-ix; 1995.

[14] D. Ferrarini, L. Vincetti, M. Zoboli, A. Cucinotta, and S. Selleri, “Leakage properties of photonic crystal fibers,” Optics Express, vol. 10, no. 23, pp.1314-1319, 2002.

[15] G. P. Agrawal, “Nonlinear Fiber Optics,” Academic Press, 2nd Edition, 1995.

[16] S. Sjolander and C. Urbaniczky, “Integrated fluid handling system for bio-molecular interaction analysis.” Analytical Chemistry vol. 63, pp. 2338-2345,1991.

[17] Y. Hibino and H. Hanafusa, “Defect structure and formation mechanism of drawing induced absorption at 630 nm in silica optical fibers,” J. Appl. Phys. Vol. 60, pp. 1797,1986.

[18] M. A. Habib and M. S. Anower, "A Novel Low Loss Porous-Core Photonic Crystal Fiber for Terahertz Wave Transmission," in International Conference on Electrical, Computer and Communication Engineering (ECCE), Cox’s Bazar, Bangladesh, 2017.

[19] L. Chaudhary, A. Jb, and H. Purohit, “Photonic Crystal Fibre : Developments , Properties and Applications in Optical Fiber Communication,” International Journal for Research in Applied Science & Engineering Technology (IJRASET), vol. 5, no. Xi, pp. 1828–1832, 2017.

[20] R. Islam, G. K. M. Hasanuzzaman, M. S. Habib, S. Rana, and M. A. G. Khan, “Low-loss rotated porous core hexagonal single-mode fiber in THz regime,” Opt. Fiber Technol., vol. 24, pp. 38–43, 2015.

[21] I. K. Yakasai, A. Rahman, P. E. Abas, and F. Begum, “Theoretical Assessment of a Porous Core Photonic Crystal Fiber for Terahertz Wave Propagation,” Opt. Commun., pp. 1–11, 2018.

[22] J. Sultana et al., “Highly birefringent elliptical core photonic crystal fiber for terahertz application,” Opt. Commun., vol. 407, pp. 92–96, 2017.

[23] S. Ali et al., “Guiding properties of a hybrid core porous fiber (HCPF) for terahertz wave propagation,” 2nd International Conference on Electrical, Computer & Telecommunication Engineering (ICECTE), 2016, Rajshahi-6204, Bangladesh.

[24] M. R. Hasan, S. Ali, and S. A. Emi, “Ultra-low material loss microstructure fiber for terahertz guidance,” Photonics Lett. Pol., vol. 9, no. 2, pp. 66–68, 2017.

[25] Archenault, M., Gagnaire, H., Goure, J. P. and Jaffrezic-Renault, N., "A simple intrinsic optical fibre refractometer," Sensors and Actuators B: Chemical 5(1-4), 173-179 ,1991.

[26] Egami, C., Takeda, K., Isai, M. and Ogita, M., "Evanescent-wave spectroscopic fiber optic pH sensor," Optics Communications 122(4-6), 122-126 ,1996.

[27] Trolier-McKinstry, S., Fox, G. R., Kholkin, A., Muller, C. A. P. and Setter, N., "Optical fibers with patterned ZnO/electrode coatings for flexural actuators " Sensors and Actuators A: Physical 73(3), 267-274 ,1999.

[28] Yuan, J. and El-Sherif, M. A., "Fiber-optic chemical sensor using polyaniline as modified cladding material," IEEE Sensors 3(1), 5-12 ,2003.

[29] Guo, H. and Tao, S., "An active core fiber-optic temperature sensor using an Eu(III)-doped sol-gel silica fiber as a temperature indicator," IEEE Sensors Journal 7(6), 953-954 ,2007.

[30] MacCraith, B. D., McDonagh, C. M., O'Keeffe, G., McEvoy, A. K., Butler, T. and Sheridan, F. R., "Sol-gel coatings for optical chemical sensors and biosensors," Sensors and Actuators B: Chemical 29(1-3), 51-57 ,1995.

[31] Soloman, S., [Sensors Handbook], McGraw Hill 245-246 ,2009.

[32] Yin, S., [Fiber optic sensors], 2nd edn, Taylor & Francis Group, CRC Press ,2008.

[33] Fuhr, P. L., "Measuring with light (in four parts)," Sensors Magazine, San Jose, CA,2000.

[34] Patrick, H. J., Kersey, A. D. and Bucholtz, F., "Analysis of the response of long period fiber gratings to external index of refraction," Journal of light wave technology 16(9), 1606-1612 ,1998.

[35] Iadicicco, A., Cusano, A., Campopiano, S., Cutolo, A. and Giordano, M., "Thinned fiber Bragg grating as refractive index sensors," IEEE Sensors Journal 5(6), 1288-1295 ,2005.

[36] Iadicicco, A., Campopiano, S., Cutolo, A., Giordano, M. and Cusano, A., "Refractive index sensor based on micro-structured fiber Bragg grating," IEEE Photonics Technology Letters 17(6), 1250-1252 ,2005.

[37] Culshaw, B., Muhammad, F., Stewart, G., Murray, S., Pinchbeck, D., Norris, J., Cassidy, S., Wilkinson, M., Williams, D., Crisp, I., Van Ewyk, R. and McGhee, A., "Evanescent wave methane detection using optical fibres," Electronics Letters 28(24), 2232-2234 ,1992.

[38] Cox, F. M., Lwin, R., Large, M. C. J. and Cordeiro, C. M. B., "Opening up optical fibres," Optics Express 15(19), 11843-11848 ,2007.

[39] Newby, K., Reichert, W. M., Andrade, J. D. and Benner, R. E., "Remote spectroscopic sensing of chemical absorption using a single multimode optical fiber," Applied Optics 23(11), 1812-1815 ,1984.

[40] Allsop, T., Reeves, R., Webb, D. J., Bennion, I. and Neal, R., "A high sensitivity refractometer based upon a long period grating Mach-Zehnder interferometer," Review of Scientific Instruments(73), 1702-1705 ,2002.

[41] Kurihara, K., Ohkawa, H., Iwasaki, Y., Niwa, O., Tobita, T. and Suzuki, K., "Fiber-optic conical microsensors for surface plasmon resonance using chemically etched single-mode fiber," Analytica Chimica Acta 523(2), 165-170 ,2004.

[42] Chiu, M. H., Wang, S. F. and Chang, R. S., "D-type fiber biosensor based on surface-plasmon resonance technology and heterodyne interferometry," Optics Letters 30(3), 233-235 ,2005.

[43] Asawa, C. K., Yao, S. K., Stearns, R. C., Mota, N. L. and Downs, J. W., "High-sensitivity fibre-optic strain sensors for measuring structural distortion," Electronics Letters 18(9), 362-364 ,1982.

[44] Lagakos, N., Cole, J. H. and Bucaro, J. A., "Microbend fiber-optic sensor," Applied Optics 26(11), 2171-2180 ,1987.

[45] Lee, S. T., Aneeshkumar, B., Radhakrishnan, P., Vallabhan, C. P. G. and Nampoori, V. P. N., "A microbent fibre optic pH sensor," Optics Communications 205(4-6), 253-256 ,2002.

[46] Pandey, N. K. and Yadav, B. C., "Embedded fibre optic microbend sensor for measurement of high pressure and crack detection," Sensors and Actuators A: Physical 128(1), 33-36 ,2006.

[47] Luo, F., Liu, J., Ma, N. and Morse, T. F., "A fiber optic microbend sensor for distributed sensing application in the structural strain monitoring," Sensors and Actuators A: Physical 75(1), 41-44 ,1999.

[48] MacLean, A., Moran, C., Johnstone, W., Culshaw, B., Marsh, D. and Parker, P., "Detection of hydrocarbon fuel spills using a distributed fibre optic sensor," Sensors and Actuators A: Physical 109(1-2), 60-67 ,2003.

[49] Nath, P., Singh, H. K., Datta, P. and Sarma, K. C., "All-fiber optic sensor for measurement of liquid refractive index," Sensors and Actuators A: Physical 148(1), 16-18 ,2008.

[50] Ilev, I. K. and Waynant, R. W., "All-fiber-optic sensor for liquid level measurement," Review of Scientific Instruments 70(5), 2551-2554 ,1999.

[51] Komachiya, M., Fumino, T., Sakaguchi, T. and Watanabe, S., "Design of a sensing glass fiber with specific refractive-index composition for a system with 1.3 μm wavelength light source," Sensors and Actuators A: Physical 78(2), 172-179 ,1999.

[52] Otsuki, S., Adachi, K. and Taguchi, T., "A novel fiber-optic gas-sensing configuration using extremely curved optical fibers and an attempt for optical humidity detection," Sensors and Actuators B: Chemical 53(1-2), 91-96 ,1998.

[53] Yeo, T. L., Sun, T. and Grattan, K. T. V., "Fibre-optic sensor technologies for humidity and moisture measurement," Sensors and Actuators A: Physical 144(2), 280-295 ,2008.

[54] Viets, C. and Hill, W., "Fibre-optic SERS sensors with angled tips," Journal of Molecular Structure 565-566(1-3), 515-518 ,2001.

[55] Lucotti, A. and Zerbi, G., "Fiber-optic SERS sensor with optimized geometry," Sensors and Actuators B: Chemical 121(2), 356-364 ,2007.

[56] Kostovski, G., White, D. J., Mitchell, A., Austin, M. W. and Stoddart, P. R., "Nanoimprinted optical fibres: Biotemplated nanostructures for SERS sensing," Biosensors and Bioelectronics 24(5), 1531-1535 ,2008.

[57] Zhang, Y., Gu, C., Schwartzberg, A. M. and Zhang, J. Z., "Surface-enhanced Raman scattering sensor based on D-shaped fiber," Applied Physics Letters 87(12), 123105-123103 ,2005.

[58] Jorgenson, R. C. and Yee, S. S., "A fiber-optic chemical sensor based on surface plasmon resonance," Sensors and Actuators B: Chemical 12(3), 213-220 ,1993.

[59] Trouillet, A., Ronot-Trioli, C., Veillas, C. and Gagnaire, H., "Chemical sensing by surface plasmon resonance in a multimode optical fibre," Pure and Applied Optics 5(2), 227-237 ,1996.

[60] Piliarik, M., Homola, J., Manikova, Z. and Ctyroky, J., "Surface plasmon resonance sensor based on a single-mode polarization-maintaining optical fiber," Sensors and Actuators B: Chemical 90(1-3), 236-242 ,2003.

[61] Tubb, A. J. C., Payne, F. P., Millington, R. B. and Lowe, C. R., "Single-mode optical fiber surface plasma wave chemical sensor," Sensors and Actuators B: Chemical 41(1-3), 71-79 ,1997.

[62] Keith Refson, "Introduction to DFT and the plane-wave pseudo potential method," Science and Technologies Facilities Council, pp. 1–55, Apr. 2014.

[63] Stig E Barkou Libori, "Photonic Crystal Fiber- From theory to practice," Ph.D thesis, Technical University of Denmark, Denmark, Feb. 2002.

[64] Ray W. Clough and Edward L. Wilson, "Early Finite Element Research at Berkeley," in the Fifth U.S. National Conference on Computational Mechanics, pp. 1–35, Aug. 1999.

[65] Fernando L. Teixeira, "Time-Domain Finite-Difference and Finite-Element Methods for Maxwell Equations in Complex Media," IEEE TRANSACTIONS ON ANTENNAS AND PROPAGATION, vol. 56, no. 8, pp. 2150-2166, Aug. 2008.

[66] Jo-Yu Wu and Robert Lee, "The Advantages of Triangular and Tetrahedral Edge Elements for Electromagnetic Modeling with the Finite-Element Method," IEEE TRANSACTIONS ON ANTENNAS AND PROPAGATION, vol. 45, no. 9, pp. 1431-1437, Sep. 1997.

[67] Biacore AB BIACORE Technology Handbook. ,1994.

[68] Kretschmann, E. and Reather, H. Radiative decay of nonradiative surface plasmon excited by light. Z.Naturf. 23A: 2135-2136; 1968.

[69] Kretschmann, E. Die Bestimmung optischer Konstanten von Metallen durch Anregung von Oberflachenplasmaschwingugnen. Z Phys 241: 313-324; 1971.

[70] Otto, A. Exitation of nonradiative surface plasma waves in silver by the method of frustrated total reflection. Z Phys 216: 398-410; 1968.

[71] Pockrand, I. et al Surface plasmon spectroscopy of organic monolayer assemblies. Surface Sci. 74: 237-244; 1978.

[72] Peterlinz, K. A. and Georgiadis, R. Two-color approach for determination of thickness and dielectric constant of thin films using surface plasmon resonance. Opt.Commun. 130: 260-266; 1996.

[73] Liedberg, B. et al Principles of biosensing with an extended coupling matrix and surface plasmon resonance. Sensors and Actuators B 11: 63-72; 1993.

[74] Zhang, L. and Uttamchandani, D. Optical chemical sensing employing surface plasmon resonance. Electron Lett. 23: 1469-1470; 1988.

[75] Striebel, Ch. et al Characterization of biomembranes by spectral elipsometry, surface plasmon resonance and interferometry with regard to biosensor application. Biosens.Bioelectron. 9: 139-146; 1994.

[76] Lofas, S. and Johnsson, B. A novel hydrogel matrix on gold surfaces in surface plasmon resonance sonsors for fast en efficient covalent immobilization of ligands. J.chem.soc., chem commun. 1526-1528; 1990.

[77] Lofas, S. Dextran modified self-assembled monolayer surfaces for use in biointeraction analysis with surface plasmon resonance. Pure & Appl.Chem. 67: 829-834; 1995.

[78] S. Lofas et al "Bioanalysis with surface plasmon resonance." Sensors and Actuators B vol. 5, pp. 79-84,1991.

[79] R. Karlsson et al "Kinetic analysis of monoclonal antibody-antigen interactions with a new biosensor based analytical system." Journal of Immunological Methods 229-240; 1991.

[80] P. Safsten et al, "Screening antibody-antigen interactions in parallel using Biacore A100." Analytical Biochemistry ,2006.

[81] B.D. Gupta and A.K. Sharma,"Sensitivity evaluation of a multi-layered surface plasmon resonance-based fiber optic sensor: A theoretical study."Sens. Actuators B Chem., vol. 107, no. 9, pp. 40–46,2005.

[82] K.M. Mc Peak, S.V. Jayanti, S.J. Kress, S. Meyer, S. Iotti, and A. Rossinelli, "Plasmonic films can easily be better: Rules and recipes." ACS Photonics, vol. 2, pp. 326–333, 2015.

[83] Y. Lu, C.J. Hao, B.Q. Wu, M. Musideke, L.C. Duan, W.Q. Wen, and J.Q. Yao, "Surface plasmon resonance sensor based on polymer photonic crystal fibers with metal nano layers." Sensors, vol. 13, pp. 956–965, 2013.

[84] B. D. Gupta and R. K. Verma, Surface Plasmon Resonance-Based Fiber Optic Sensors: Principle, Probe Designs, and Some Applications, Journal of Sensors, 2009,1-12,2009.

[85] Zamarreño, C. R., Rivero, P. J., Hernaez, M., Goicoechea, J., Matías, I. R., & Arregui, F. J. Optical Sensors for Corrosion Monitoring. Intelligent Coatings for Corrosion Control, 603–640 ; 2015.

[86] Descrovi, E., Paeder, V., Vaccaro, L., & Herzig, H.-P. A virtual optical probe based on localized Surface Plasmon Polaritons. Optics Express, 13(18), 7017. doi:10.1364/opex.13.007017, 2005.

[87] Anderson, G. P., & Taitt, C. R. EVANESCENT WAVE FIBER OPTIC BIOSENSORS. Optical Biosensors, 83–138, 2008.

[88] Ligler, F. S. and Taitt, C. R. (eds), Optical biosensors: today and tomorrow, Elsevier Science, 2008.

[89] Raether, H., [Surface plasmons on smooth and rough surfaces and on gratings], Springer, New York, 1988.

[90] Ritchie, R. H., Arakawa, E. T., Cowanand, J. J. and Hamm, R. N., "Surface plasmon resonance effect in grating diffraction," Physical Review Letters 21(22), 1530-1533 ,1968.

[91] Barnes, W. L., Murray, W. A., Dintinger, J., Devaux, E. and Ebbesen, T. W., "Surface plasmon polaritions and their role in the enhanced transmission of light through periodic arrays of subwavelength holes in a metal film," Physical Review Letters 92(10), 107401 ,2004.

[92] Sharma, A. K, Jha, R. and Gupta, B. D., "Fiber-optic sensors based on surface plasmon resonance: a comprehensive review," IEEE Sensors 7(8), 1118-1129 ,2007.

[93] Fan, X., White, I. M., Shopova, S. I., Zhu, H., Suter, J. D. and Sun, Y., "Sensitive optical biosensors for unlabeled targets: a review," Analytica Chimica Acta 620(1-2), 8-26 ,2008.

[94] Wolfbeis, O. S., "Fiber-optic chemical sensors and biosensors," Analytical Chemistry 80(12), 4269-4283 ,2008.

[95] Lee, B., Roh, S. and Park, J., "Current status of micro- and nano-structured optical fiber sensors," Optical Fiber Technology 15(3), 209-221 ,2009.

[96] Homola, J., "Optical fiber sensor based on surface plasmon excitation," Sensors and Actuators B: Chemical 29(1-3), 401-405 ,1995.

[97] Tseng, S. M., Hsu, K. Y., Wei, H. S. and Chen, K. F., "Analysis and experiment of thin metal-clad fiber polarizer with index overlay," IEEE Photonics Technology Letters 9(5), 628-630 ,1997.

[98] Esteban, O., Alonso, R., Navarrete, M. C. and Cano, A. G., "Surface plasmon excitation in fiber-optics sensors: a novel theoretical approach," Journal of lightwave technology 20(3), 448-453 ,2002.

[99] Lin, G. C., Wang, L., Yang, C. C., Shih, M. C. and Chuang, T. J., "Thermal performance of metal-clad fiber Bragg grating sensors," IEEE Photonics Technology Letters 10(3), 406-408 ,1998.

[100] Schroeder, K., Ecke, W., Mueller, R., Willsch, R. and Andreev, A., "A fibre Bragg grating refractometer," Measurement Science and Technology 12(7), 757-764 ,2001.

[101] Sharma, A. K and Gupta, B. D., "Fiber optic sensor based on surface plasmon resonance with nanoparticle films," Photonics and Nanostructures - Fundamentals and Applications 3(1), 30-37 ,2005.

[102] Sharma, A. K and Gupta, B. D., "Fiber-optic sensor based on surface plasmon resonance with Ag-Au alloy nanoparticle films," Nanotechnology 17(1), 124-131 ,2006.

[103] R. Hasan, S. Akter, A. A. Rifat, S. Rana, and S. Ali, “A Highly Sensitive Gold-Coated Photonic Crystal Fiber Biosensor Based on Surface Plasmon Resonance” Photonics, vol. 4, no. 4, pp. 18 ,2017.

[104] A. Vial, A. Grimault, and D. Barchiesi, “Improved Analytical Fit of Gold Dispersion: Application to the Modeling of Extinction Spectra with a Finite-Difference Time-Domain Method,” Physical Review B, vol. 71, no.8, pp. 1–7, 2005.

[105] J. Sultana et al., “Dual-Polarized Highly Sensitive Plasmonic Sensor in the Visible to Near-IR Dual-polarized highly sensitive plasmonic sensor in the visible to near-IR spectrum,” Optics Express, vol. 26, no. 23, pp. 30347- 30361, 2018.

[106] M. A. Mollah, A. K. Paul and S. M. A. Razzak “Surface Plasmon Resonance based Dual-Polarized Photonic Crystal Fiber Refractive Index Sensor,” 2018 Int. Conf. Adv. Electr. Electron. Eng., pp. 1–4, 2018, Gazipur, Bangladesh.

[107] A. A. Rifat, R. Ahmed, G. A. Mahdiraji, and F. R. M. Adikan, “Highly Sensitive D-Shaped Photonic Crystal Fiber Based Plasmonic Biosensor in Visible to Near-IR,” IEEE Sensors Journal, vol. 17, no. 9, pp. 2776–2783, 2017

[108] A. A. Rifat et al., “Photonic Crystal Fiber-Based Surface Plasmon Resonance Sensor with Selective Analyte Channels and Graphene-Silver Deposited Core,” Sensors, vol. 15, no. 5 pp. 11499–11510, 2015.

[109] R. K. Gangwar and V. K. Singh, “Highly Sensitive Surface Plasmon Resonance Based D-Shaped Photonic Crystal Fiber Refractive Index Sensor,” Plasmonics, vol. 12, no. 5, pp. 1–6, 2016.

[110] A. A. Rifat, G. A. Mahdiraji, Y. M. Sua, Y. G. Shee, R. Ahmed, D. M. Chow, & F. R. M. Adrikan,” Surface Plasmon Resonance Photonic Crystal Fiber Biosensor: A Practical Sensing Approach,” IEEE Photonics Technology Letters, vol.27, no. 15, pp. 1628–1631, 2015.

[111] Chao Liu et al., “Mid-infrared surface plasmon resonance sensor based on photonic crystal fibers,” Optics Express, vol. 25, no. 13, pp. 8427–8432, 2017.

[112] A. Ullah, M. M. S. Hossain, and M. S. Alam, “SPR Biosensor Based on Microstructured Fiber with Lens Shaped Air Holes,” 2017 IEEE International Conference on Telecommunications and Photonics (ICTP), pp. 26–28, 2017, Dhaka, Bangladesh.

[113] B. O. Liedberg, Claes Nylander and Ingemar Lundstrom, “Surface plasmon resonance for gas detection and biosensing*,” Sensors and Actuators, vol. 4, pp. 299–304, 1983.

[114] S. Chakma, A. Khalek, B. K. Paul, R. Hasan, and A. N. Bahar, “Gold-Coated Photonic Crystal Fiber Biosensor based on Surface Plasmon Resonance: Design and Analysis,” Sensing and Bio-Sensing Research, vol. 18, pp. 7-12, 2018.

[115] S. Islam et al., “A Hi-Bi Ultra-Sensitive Surface Plasmon Resonance Fiber Sensor,” IEEE Access, vol. 7, pp. 79085–79094, 2019.

[116] S. Sharmin, A. Bosu and S. Akhtar, “A Simple Gold-Coated Photonic Crystal Fiber Based Plasmonic Biosensor,” 2018 International Conference on Advances in Electronics Engineering, pp. 1–4, 2018, Gazipur, Bangladesh.

[117] J. N. Dash and R. Jha, “SPR Biosensor Based on Polymer PCF Coated With Conducting Metal Oxide,” IEEE Photonics Technology Letters, vol. 26, no. 6, pp. 595–598, 2014.

[118] S. S. Yee, Jir'ı´ Homola and Gu¨ nter Gauglitz “Surface plasmon resonance sensors: review,” Sensors and Actuators, vol. 54, pp. 3–15, 1999.

[119] S. Chu et al., “Design and Analysis of Surface Plasmon Resonance based Photonic Quasi-Crystal Fibre Biosensor for High Refractive Index Liquid Analytes,” EEE Journal of Selected Topics in Quantum Electronics, vol. 25, no. 2 , pp. 1–8, 2018.

[120] M. R. Momota, & Hasan, M. R. Hasan, “Hollow-core silver coated photonic crystal fiber plasmonic sensor,” Optical Materials, vol. 76, pp. 287–294, 2018.

[121] M. A. Mollah, A. K. Paul, and S. M. A. Razzak, “Dual Polarized Plasmonic Refractive Index Sensor based on Photonic Crystal Fiber,” 2018 10th International Conference on Computer and Electrical Engineering, pp. 73–76, 2018.

[122] R. Hasan et al., “Spiral Photonic Crystal Fiber-Based Dual-Polarized,” IEEE Sensors Journal, vol. 18, no. 1, pp. 133–140, 2018.

[123] A. Rifat, F. Haider, R. Ahmed, G. A. Mahdiraji, F. R. M. Adikan, and A. E. Miroshnichenko, “Highly sensitive selectively coated photonic crystal fiber-based plasmonic sensor,” Optics letters, vol. 43, no. 4, pp. 891–894, 2018.

[124] G. Wang, S. Li, G. An, X. Wang, Y. Zhao, and W. Zhang, “Highly sensitive D-shaped photonic crystal fiber biological sensors based on surface plasmon resonance,” Optical Quantum Electronics., vol. 48, no. 1, pp. 1–9, 2016.

[125] Min Liu, Hongtao Yuan, Ping Shun and Xu. Yang, “High-sensitivity birefringent and single-layer coating photonic crystal fiber biosensor based on surface plasmon resonance,” Applied Optics, vol. 57, no. 8, pp. 1883–1886, 2018.

[126] A. A. Rifat, G. A. Mahdiraji, Y. G. Shee, J. Shawon, and F. R. Mahamd, " A Novel Photonic Crystal Fiber Biosensor Using Surface Plasmon Resonance,” Procedia Engineering, vol. 140, pp. 1–7, 2016.

[127] E. Haque, A. Hossain, F. Ahmed, and Y. Namihira, “Surface Plasmon Resonance Sensor Based on Modified D -Shaped Photonic Crystal Fiber for Wider Range of Refractive Index Detection,” IEEE Sensors Journal, vol. 18, no.20, pp. 8287 - 8293, 2018.

[128] S. Islam, J. Sultana, A. Dinovitser, Brian W.-H. Ng, and D. Abbott, “A gold coated plasmonic sensor for biomedical and biochemical analyte detection,” 43rd International Conference on Infrared, Millimeter, and Terahertz Waves (IRMMW-THz), pp. 9–10, Nagoya Congress Center, Japan, 2018.

[129] A. K. Paul, A. Bakar, S. Rahman, S. M. A. Razzak, and A. K. Sarkar, “Hybrid Cladding Structured Gold Coated Photonic Crystal Fiber Biosensor Based on Surface Plasmon Resonance,” 2nd International Conference on Electrical & Electronic Engineering (ICEEE), pp. 1–4, Rajshahi, Bangladesh, December, 2017.

[130] R. Hasan, S. Akter, A. A. Rifat, S. Rana, and S. Ali, “A Highly Sensitive Gold-Coated Photonic Crystal Fiber Biosensor Based on Surface Plasmon Resonance” Photonics, vol. 4, no. 4, pp. 18 2017.

[131] M. S. Islam, Slam, J. Sultana, R. A. Aoni, M. S. Habib, A. Dinovitser, Brian W.-H. NG, and D. Abott, "Localized surface plasmon resonance biosensor : an improved technique for SERS response intensification," Optics Letters, vol. 44, no. 5, pp. 1134–1137, 2019.

[132] E. K. Akowuah, T. Gorman, H. Ademgil, S. Haxha "A highly sensitive photonic crystal fibre (PCF) surface plasmon resonance (SPR) sensor based on a bimetallic structure of gold and silver," 2012 IEEE 4th International Conference on Adaptive Science & Technology (ICAST), Kumasi, Ghana, December, 2012

[133] J. N. Dash and R. Jha, "Graphene Based Birefringent Photonic Crystal Fiber Sensor Using Surface Plasmon Resonance," IEEE Photonics Technology Letters, vol. 26, no. 11, pp. 1092-1095, 2014.

[134] J. N. Dash and R. Jha, "Graphene Based Birefringent Photonic Crystal Fiber Sensor Using Surface Plasmon Resonance," Plasmonics, vol. 11, no. 6, pp. 1505-1509, 2014.

[135] C. Liu et al., "Symmetrical dual D-shape photonic crystal fibers for surface plasmon resonance sensing," Optics Express, vol. 26, no. 7, pp. 481–490, 2018.

[136] R. H. Ritchie, Plasma Losses by Fast Electrons in Thin Films, Phys. Rev. 106, 874, 1957.

[137] Ahmmed, R., Ahmed, R., & Razzak, S. A. Design of large negative dispersion and modal analysis for hexagonal, square, FCC and BCC photonic crystal fibers. Paper presented at the Informatics, Electronics & Vision (ICIEV), 2013.

[138] Rifat Ahmmed Aoni, Rajib Ahmed, and S. M. Abdur Razzak, Design and Simulation of Duel-Concentric-Core Photonic Crystal Fiber for Dispersion Compensation, CIOMP-OSA Summer Session on Optical Engineering, Design and Manufacturing, 2013.

[139] Slavík, R., Homola, J., & Čtyroký, J. Single-mode optical fiber surface plasmon resonance sensor. Sensors and Actuators B: Chemical, 54(1), 74-79, 1999.

[140] Shigeru Toyama,Akira Ohide,Fedosseeva Olga, Applications of Surface Plasmon Resonance Sensor in Medical Field, IEEJ Transactions on Sensors and Micromachines 121(8):430-433, 2001.

[141] Sara Tombelli, Maria Minunni, Marco Mascini, Ronghui Wang, Improved surface plasmon resonance sensor for DNA sensing, Conference: Sensors and Microsystems - 8th Italian Conference, 2004.

[142] Dominic Siedhoff, Martin Strauch, Victoria M. Shpacovitch, Dorit Merhof, Unsupervised Data Analysis for Virus Detection with a Surface Plasmon Resonance Sensor, Image Processing, Theory and Applications (IPTA) At: Montréal, Canada, 2017.

[143] Kirill Tomyshev, Diana Tazhetdinova, Egor Manuylovich, Oleg Butov, High-resolution fiber optic surface plasmon resonance sensor for biomedical applications, Journal of Applied Physics 124(11):113106, 2018.

[144] Xue Tianyu, Weiyuan Liang, Yawen Li, Yuanhui Sun, Y. J. Xiang, Yupeng Zhang, Zhigao Dai, Yanhong Duo, Leiming Wu, Kun Qi, Dr. Shivananju B N, Lijun Zhang, Xiaoqiang Cui, Han Zhang, Qiaoliang Bao, Ultrasensitive detection of miRNA with an antimonene-based surface plasmon resonance sensor, Researchgate,2019.

[145] Haidar Jalal Ismail, Theoretical Investigation of Diabetic Urine Detection by Surface Plasmon Resonance Sensor, Optimization Biosensors, 2018

[146] Shpacovitch Victoria, Application of Surface Plasmon Resonance (SPR) for the Detection of Single Viruses and Single Biological Nano-objects, Journal of Bacteriology & Parasitology 03(07), 2012.

[147] Nancy Tawil, Edward Sacher, Rosemonde Mandeville, Michel Meunier, Surface plasmon resonance detection of E. coli and methicillin-resistant S. Aureus using bacteriophages, Biosensors & Bioelectronics 37(1):24-9, 2012.

[148] Qiaohui Luo, Neng Yu, Chunfei Shi, Xiaoping Wang, Jianmin Wu, Surface plasmon resonance sensor for antibiotics detection based on photo-initiated polymerization molecularly imprinted array, Talanta 161, 2016.

[149] Chen Zhou, Haimin Zou, Ming Li, Chengjun Sun, Dongxia Ren, Yong-Xin Li, Fiber Optic Surface Plasmon Resonance Sensor for Detection of E. coli O157:H7 based on Antimicrobial Peptides and AgNPs-rGO, Biosensors & Bioelectronics 117, 2018.

[150] Jin Wang, Masaki Muto, Rui Yatabe, Yusuke Tahara, Takeshi Onodera, Masayoshi Tanaka, Mina Okochi Kiyoshi Toko, Highly Selective Rational Design of Peptide-Based Surface Plasmon Resonance Sensor for Direct Determination of 2,4,6-trinitrotoluene (TNT) Explosive, Sensors and Actuators B: Chemical,264, 279-284, 2018.

[151] Wenhua Wang, Xinlei Zhou, Shengxu Wu, Sidong Li, Weina Wu, Zhengye Xiong, Wenqing Shi, Xiuyun Tian, Qingxu Yu, Reusable surface plasmon resonance sensor for

rapid detection of Cu^{2+} based on modified-chitosan thin film as an active layer, Sensors and Actuators A: Physical, 286, 59-67, 2019.

[152] Sushil Kumar, Gaurav Sharma, VivekSingh, Modelling of surface plasmon resonance sensor for detection of mass concentration of ethanol and methanol in a binary mixture, Infrared Physics & Technology, 67, Pages 190-196, 2014.

[153] Aslı Göçenoğlu Sarıkaya, Bilgen Osman, Tülay Çam, Adil Denizli, Molecularly imprinted surface plasmon resonance (SPR) sensor for uric acid determination, Sensors and Actuators B: Chemical, 251, 763-772, 2017.

[154] Thi-Dung Tran, Moonil Kim, A Surface Plasmon Resonance Sensor for Detection of Toluene ($C_6H_5CH_3$), Applied Science and Convergence Technology 2018; 27(6): 184-188, 2018.

[155] Takeshi Onodera, Haoyu Luo, Miaomiao Ma, Rui Yatabe, Kiyoshi Toko, Detection of Furfural Using Surface Plasmon Resonance Sensor with Indirect Competitive Method, IEEJ Transactions on Sensors and Micromachines 137(4):121-122, 2017.

[156] K. Nanameki, S. Kamata, Determination of benzethonium by using a surface plasmon resonance sensor, Japanese Journal of Forensic Toxicology 18(3):253-260, 2000.

[157] J. B. Maurya, Y. K. Prajapati, S. Raikwar, J. P. Saini, A silicon-black phosphorous based surface plasmon resonance sensor for the detection of NO_2 gas, Optik,160, 428-433, 2018.

[158] Geoffrey J Ashwell, M.P.S. Roberts, Highly Selective Surface Plasmon Resonance Sensor for NO2, Electronics Letters 32(22):2089 – 2091, 1996.

[159] Amal Ibrahim Mahmood, Design and Simulation of Surface Plasmon Resonance Sensors for Environmental Monitoring, Conference: IHSCICONF2017, 2018.

[160] Vladimir Chegel, Yu.M Shirshov, E.V Piletskaya, Sergey A Piletsky, Surface plasmon resonance sensor for pesticide detection, Sensors and Actuators B Chemical 48(1):456-460, 1998.

[161] Jean-Francois Masson, Saome Banerji, Yoon-Chang Kim,Karl S. Booksh, Surface plasmon resonance sensors for industrial applications, Proceedings of SPIE - The International Society for Optical Engineering 5586, 2004.

[162] Jiangcai Wang, Weihua Lin, En Cao, Xuefeng Xu, Wenjie Liang, Xiaofang Zhang, Surface Plasmon Resonance Sensors on Raman and Fluorescence Spectroscopy, Sensors 17(12):2719, 2017.

[163] Jinru Zhou, Qinqin Qi, Chong Wang, Yifan Qian, Guangming Liu, Yanbo Wang, Linglin Fu, Surface plasmon resonance (SPR) biosensors for food allergen detection in food matrices, Biosensors and Bioelectronics, 142, 111449, 2019.

[164] Nurul Hida Zainuddin, Yap Wing Fen, Ali Abdul Khaleq Al Wahib, Mohd Hanif Yaacob, Noriah Bidin , Nur Alia Sheh Omer, Mohd Adzir Mahdi, Detection of adulterated honey by surface plasmon resonance optical sensor, Optik, 168, 134-139, 2018.

[165] C Mouvet, R. D. Harris, C. Maciag, B.J.Luff, J.S. Wilkinson, J. Piehler, A. Brecht, G. Gauglitz, R. Abuknesha, G. Ismail, Determination of simazine in water samples by waveguide surface plasmon resonance, Analytica Chimica Acta, 338, 1–2,1997

[166] Yuzhi Chen, Yongqin Yu, Xuejin Li, Zhixin Tan, Youfu Geng, Experimental Comparison of Fiber-Optic Surface Plasmon Resonance Sensors with Multi Metal Layers and Single Silver or Gold Layer, Plasmonics 10,6, 2015.

[167] M.R. Hasan, M.I. Hasan, M.S. Anower, Tellurite glass defectcore spiral photonic crystal fiber with low loss and large negative flattened dispersion over S+C+L+U wavelength bands, Appl. Opt. 54, 9456–9461, 2015.

[168] E.K. Akowuah, T. Gorman, H. Ademgil, S. Haxha, G.K. Robinson, J.V. Oliver, Numerical analysis of a photonic crystal fiber for biosensing applications, IEEE J. Quantum Electron. 48, 1403–1410, 2012.

[169] MD. SAIFUL ISLAM, CRISTIANO M. B. CORDEIRO, JAKEYA SULTANA, RIFAT AHMED AONI, SHILUN FENG, RAJIB AHMED, MOHSEN DORRAKI, ALEX DINOVITSER, BRIAN W.-H. NG, AND DEREK ABBOTT, A Hi-Bi Ultra-Sensitive Surface Plasmon Resonance Fiber Sensor, IEEE Access, 2019.

[170] Md. Nazmul Hossen, Md. Ferdous, Md. Abdul Khalek, Sujan Chakma, Bikash Kumar Paul, Kawsar Ahmed, Design and analysis of biosensor based on surface plasmon resonance, Sensing and Bio-Sensing Research 21, 1-6, 2018.

[171] Md. Saiful Islam, Mohammad Rakibul Islam, Jakeya Sultana, Alex Dinovitser, Brian W. -H. Ng, Derek Abbott, Exposed core localized surface plasmon resonance biosensor, Journal of OSA B,36,8, 2019.

[172] Md. Rabiul Hasan, Sanjida Akter, Ahmmed A. Rifat, Sohel Rana, Kawsar Ahmed, Rajib Ahmed, Harish Subbaraman, and Derek Abbott, Spiral Photonic Crystal Fiber-Based Dual-Polarized Surface Plasmon Resonance Biosensor, IEEE Sensors Journal-18, 2018.

[173] Alok Kumar Paul, Ajay krishno Sarkar, Abu Bakar Siddiqur Rahman and Abdul Khaleque, Twin Core Photonic Crystal Fiber Plasmonic Refractive Index Sensor, IEEE Sensors Journal, 2018.

[174] Md. Ekhlasur Rahaman, Rekha Shaha, Md. Shamim Ahsan, Ik-Bu Sohn, Design and Performance Analysis of a D-shaped PCF and Surface Plasmon Resonance Based Glucose Sensor, 4th international conference on Electrical Engineering and Information and Communication Technology, 2018

[175] Duanming Li, Wei Zhang, Huan Liu, Jiangfei Hu, and Guiyao Zhou, High sensitivity refractive index sensor based on multi-coating photonic crystal fiber with surface plasmon resonance at near-infrared wavelength, IEEE Photonics Journal, 2017